Amplitude and timing of the Laschamp geomagnetic dipole low from the global atmospheric 10 Be overproduction: Contribution of authigenic 10 Be/ 9 Be ratios in west equatorial Pacific sediments

L L Ménabréaz, Didier Bourles, Nicolas Thouveny

Amplitude and timing of the Laschamp geomagnetic dipole low from the global atmospheric ^{10}Be overproduction: contribution of authigenic $^{10}Be/^{9}Be$ ratios in West Equatorial Pacific sediments.

L. Ménabréaz[1], D.L. Bourlès*, and N. Thouveny**.

* Aix-Marseille Université, CNRS, IRD, CEREGE UM34, 13545 Aix-en-Provence Cedex 04, France.

[1] Corresponding author : menabreaz@cerege.fr

Abstract

Authigenic $^{10}Be/^{9}Be$ ratios were measured along a sediment core collected in the West Equatorial Pacific in order to reconstruct cosmogenic ^{10}Be production variations near the equator, where the geomagnetic modulation is maximum. From 60 to 20 ka, the single significant ^{10}Be production impulse recorded at 41 ka results from the geomagnetic dipole low that triggered the Laschamp excursion. No significant ^{10}Be overproduction signature is recorded at the age of the Mono Lake excursion (~34 ka). A compilation of authigenic $^{10}Be/^{9}Be$ records obtained from sediments was averaged over a 1 ka window and compared with the 1 ka-averaged ^{10}Be flux record of Greenland ice cores. Their remarkable similarity demonstrates that the ^{10}Be production is globally modulated by geomagnetic dipole variations and redistributed by atmosphere dynamics. After calibration using absolute values of the virtual dipole moment drawn from paleomagnetic database, the authigenic $^{10}Be/^{9}Be$ stack allows reconstructing the geomagnetic dipole moment variations over the 20-50 ka time interval. Between 48 ka and 41 ka, the dipole moment collapsed at a rate of -1.5×10^{22} $A.m^2.ka^{-1}$, which will be an interesting criterion for the assessment of the loss rate of the historical field and the comparison of dipole moment loss prior to excursions and reversals. After a 2 ka duration of the minimum dipole moment ($\sim 1 \times 10^{22}$ $A.m^2$), a slow increase started at 39 ka, progressively reaching 5×10^{22} $A.m^2$ at 20 ka. The absence of a significant dipole moment drop at 34 ka, the age of the Mono lake excursion, suggests that the duration and amplitude of the dipole weakening cannot be compared with that of the Laschamp. This study provides a reliable basis to model the production of radiocarbon and *in-situ* cosmogenic nuclides and to improve the calibration of these dating methods.

1. Introduction

The understanding of past and present geomagnetic field behaviour depends on the accuracy and precision of proxy records of geomagnetic field magnitude and direction. Since the last geomagnetic reversal (780 ka ago), the geomagnetic dipole moment appears to have been affected by repeated drops, which generate large directional variations of the geomagnetic vector field [e.g. *Thouveny et al.,* 2008; *Channell et al.,* 2009]. The interpreted global character of these geomagnetic instabilities however strongly depends on the geographic distribution of available paleomagnetic records and on the recording materials (sediments or volcanic rocks), which influence the reliability of the recorded phenomena (amplitude and duration). This is illustrated by the ongoing debate over the occurrence of one or two dipole lows / excursions during the 30-45 ka interval: Laschamp at ~41 ka and possibly Mono Lake at ~33 ka.

Quasi-reversed magnetizations recorded in Laschamp and Olby lava flows, (Massif central, France) provided the first evidence of a past transient reversed state of the geomagnetic field [*Bonhommet and Babkine,* 1967]. The first dating by *Bonhommet and Zahringer* [1969] using K/Ar methods performed on whole rock led to an age determination between 8 and 20 ka. After almost four decades of geochronologic investigations using K–Ar, thermoluminescence, $^{40}Ar/^{39}Ar$ and $^{230}Th–^{238}U$ methods [e.g. *Bonhommet and Zähringer*, 1969; *Condomines*, 1980; *Hall and York*, 1978; *Gillot et al.*, 1979; *Chauvin et al.,* 1989; *Plenier et al.,* 2007], the most reliable radiometric age datasets finally led to concordant ages of 40.4±2.0 ka [*Guillou et al.,* 2004] and 40.7±1.0

64 ka BP [*Singer et al.*, 2009]. Meanwhile, the Laschamp excursion has been identified
65 worldwide as a large amplitude swing of the magnetization vectors, and/or as a dramatic
66 paleointensity low in lava flows (e.g. *Kristjansson and Gudmundsson*, 1980; *Roperch et*
67 *al.*, 1988; *Levi et al.*, 1990; *Mochizuki et al.*, 2006; *Cassata et al.*, 2008] and sediments
68 [e.g. *Thouveny and Creer*, 1992; *Vlag et al.*, 1996; *Lund et al.*, 2005; *Channell*, 2006].
69 These studies thus established the global extension of the geomagnetic anomaly and mark
70 it as the major geomagnetic crisis to have occurred over the last 50 ka.

71 In contrast with the Laschamp case, the occurrence and/or the age of the Mono
72 Lake (ML) excursion/dipole moment low remain controversial. *Denham and Cox* [1971],
73 while seeking a record of the Laschamp excursion at Mono Lake (California), detected
74 excursional paleomagnetic directions in sedimentary layers of the Wilson Creek
75 formation. These layers were initially radiocarbon dated at ~24 ka, i.e. at an age older
76 than the age attributed at that time to the Laschamp excursion [*Bonhommet and*
77 *Zahringer*, 1969]. The ML excursion was thus considered as distinct from the Laschamp
78 excursion. It was later described in other North-Western American lacustrine sections
79 [e.g. *Negrini et al.*, 1984; *Liddicoat et al*., 1992; *Coe and Liddicoat*, 1994; *Hanna and*
80 *Verosub*, 1989] as well as North Atlantic sediments [e.g. *Novaczyk and Knies*, 2000;
81 *Channell*, 2006]. The age of the excursion in the Mono Lake sediment sequence has since
82 been revised from ~24 ka [*Denham and Cox*, 1971] to ~32 – 34 ka [*Negrini et al*., 2000;
83 *Benson et al.*, 2003; *Zic et al.* 2002]. This is, however, still subject to debate. Indeed, ^{14}C
84 ages obtained on lacustrine carbonates and $^{40}Ar/^{39}Ar$ ages of sanidine crystals from the
85 Wilson Creek Formation which range from 38 to 41 ka suggest, on the contrary, that the
86 ML excursion should be assigned to the Laschamp excursion [*Kent et al.*, 2002]. The

87 correlation of the Mono Lake RPI stack [*Zimmerman et al.*, 2006] with the GLOPIS
88 record of *Laj et al.* [2004] supports this attribution.

89 Marine sediment relative paleointensity (RPI) records however, often display two
90 successive significant RPI lows attributed to the Laschamp and Mono Lake excursions
91 [*Nowaczyk and Knies*, 2000; *Laj et al*., 2000, 2004; *Channel et al*., 2006; *Lund et al*.,
92 2006]. The Mono Lake RPI low is recorded at ~34.7 ka according to the correlation of
93 the sedimentary paleoclimatic proxies with oxygen isotopes records from Greenland
94 [GICC05 age model; *NGRIP dating group 2006*, and references therein]. Volcanic
95 records of the Mono Lake excursion were also retrieved from New Zealand [*Shibuya et*
96 *al.*, 1992; *Mochizuki et al*., 2004, 2006, 2007; *Cassata et al.*, 2008 ; *Cassidy and Hill*,
97 2009], Hawaii [*Laj et al*., 2002; *Teanby et al.*, 2002] and the Canary Islands [*Kissel et al.*,
98 2011]. The case of the Mono Lake excursion, therefore, remains controversial. Both its
99 age and the amplitude of dipole moment reduction remain uncertain.

100 Deciphering the amplitude and timing of dipole moment lows can be performed
101 using methods independent from rock- and paleomagnetism, such as those based on
102 cosmogenic nuclide production recorded in sediments and ice cores. Meteoric Beryllium-
103 10 (^{10}Be, half-life: 1.387 ± 0.012 Ma [*Chmeleff et al.*, 2010; *Korschinek et al.*, 2010]) is
104 produced through nucleonic cascades in the atmosphere which result from nuclear
105 interactions between the Galactic Cosmic Rays (GCR) and the Oxygen and Nitrogen
106 atmospheric targets. Proportional to the flux of the highly energetic charged particles
107 constituting the GCR, the ^{10}Be production rate is mainly modulated over multi-millennial
108 time scales by the variability of the magnetospheric shielding dominated by the
109 geomagnetic dipole. In appropriate archives, records of ^{10}Be production rates thus

provide proxies of the geomagnetic dipole moment variations [e.g. *Lal,* 1988]. Independent from paleomagnetic methods, this approach is particularly well suited to confirm or invalidate the worldwide character of reported paleomagnetic features. Early works by *Elsasser et al.* [1956] and *Lal* [1988] allowed establishing an inverse relationship between the globally integrated ^{10}Be atmospheric production and the dipole moment magnitude. During the last decades, this relationship has been broadly confirmed using numerical simulations based on purely physical models [*Masarik and Beer*, 1999, 2009; *Wagner et al.*, 2000b], and experimentally supported by changes of ^{10}Be depositional fluxes in ice sheets [e.g. *Muscheler et al.*, 2005] and in marine sediment [e.g. *Robinson et al.*, 1995; *Frank*, 2000; *Carcaillet et al.*, 2003, 2004a; *Christl et al*., 2003] records.

Cosmogenic nuclide production records over the time interval spanning the Laschamp and Mono Lake excursions are provided by ^{10}Be and ^{36}Cl deposition flux in polar ice [e.g *Raisbeck et al*., 1992; *Finkel and Nishiizumi*, 1997; *Yiou et al.*, 1997; *Wagner et al.*, 2000 a, b; *Muscheler et al.*, 2005] and by marine sediments using $^{230}Th_{xs}$-normalized ^{10}Be fluxes [e.g *Frank et al.*, 1997; *Christl et al.*, 2010]. Authigenic ^{10}Be/^{9}Be records recently obtained from marine sediments [e.g. *Carcaillet et al.*, 2004a, b; *Leduc et al*., 2006; *Ménabréaz et al.*, 2011] encourage further studies in other regions, especially at low latitude, where the modulation of ^{10}Be production rates by the geomagnetic dipole is maximum.

2. Environmental setting and sediment description of core MD05-2920.

The studied core MD05-2920 (36.67 m long; 2.51°S, 144.32°E; 1848 m water depth) was retrieved with a giant piston corer during the MD148-PECTEN Cruise aboard the RV/Marion Dufresne in 2005 [*Beaufort et al.,* 2005]. The coring site is located on the north coast of Papua New Guinea, in the Bismarck Sea, at ~100 km off the Sepik and Ramu Rivers estuaries (Figure 1.A). These large rivers and their tributaries drain through erodible volcanic and igneous rock formations distributed along a steep topographic profile (the altitude of these "central mountains" is > 4000 m).

The regional climate is dominated by the Asian-Australian monsoon system [*Webster et al.,* 1998; *Wang et al.,* 2003]. The sediment discharge from rivers draining the north slope of the island of New Guinea [*Milliman et al.,* 1999] is thus very considerable. This area is characterized by a very narrow continental shelf (< 5 km), incised principally by the Sepik submarine canyon extending from the river mouth to water-depths greater than 1000m [*Cresswell,* 2000]. After the vertical divergence of the surface plume at the head of the canyon, the Sepik sediments disperse along two distinct routes [*Kineke et al.,* 2000]: much of the sediment is transported down the canyon via near-bottom hyperpycnal flows, while a surface plume, driven by the New Guinean Coastal Current, transports fine sediments eastward (during the NW monsoon) and westward (during the SE monsoon) along the shelf and slope. Evidence of intermediate turbid layers also suggests distal transport along isopycnal surfaces [*Kineke et al.,* 2000]. However, the wet conditions throughout the year limit aeolian particle transport to this area, contrarily to contributions from the river inputs [*Kawahata et al.,* 2000]. This depositional setting leads to sedimentation rates on the order of tens of centimeters per ka [*Beaufort et al.,* 2005].

155 The MD05-2920 sequence presents good stratigraphic preservation and is mainly
156 composed of homogeneous (non-laminated) greyish olive clay, with dispersed
157 foraminifers and occasional black lenses of organic matter [*Beaufort et al.*, 2005]. The
158 proportion of the terrigeneous fraction in MD05-2920 core top sediments is ~70%, and
159 that of the carbonate fraction is ~25% [*Tachikawa et al.*, 2011].

160 The sedimentary elemental composition as determined by X-ray fluorescence
161 analyses [Tachikawa et al., 2011] does not present a clear glacial-interglacial variability,
162 which implies that glacial conditions have a limited influence on the hydrological cycle,
163 which is rather linked to the intertropical convergence zone.

164

165 **3. Methodology**

166 3.1 Transport correction:

167 ^{10}Be concentration in marine sediments is the result of superimposed
168 contributions. First, it depends on the atmospheric ^{10}Be flux entering the ocean and
169 reflecting its production rate in the atmosphere. ^{10}Be is primarily produced in the
170 stratosphere: this proportion was estimated at 67% by *Lal and Peters* [1967], and at 56%
171 by *Masarik and Beer* [1999]. Once produced, the particle-reactive ^{10}Be set onto aerosols
172 is integrated to the hydrological cycle and removed from the atmospheric reservoir on a
173 yearly time-scale. *Baroni et al.* [2011] calculated a ^{10}Be atmospheric residence time of ~3
174 years which is a combination of a tropospheric residence time of approximately one week
175 and a stratospheric residence time that could be as long as 6 years. This estimation is
176 slightly higher than previous ones [*Beer et al.*, 1990; *Raisbeck et al.*, 1981], and suggests,

177 according to *Heikkilä et al.* [2011], a better ^{10}Be atmospheric mixing than previously
178 assumed. The stratospheric ^{10}Be is transferred to the troposphere at mid-latitudes [e.g.
179 *Bard and Frank,* 2006]. It seems reasonable to suppose that the atmospheric transport
180 may have a negligible effect on ^{10}Be concentration in deep-sea sediments given that ^{10}Be
181 residence time in the ocean is 500 to 1000 times higher.

182 ^{10}Be content in marine sediments is also affected by oceanic reservoir effects
183 (transport, adsorption and deposition processes) that depend on Be scavenging efficiency,
184 residence time and particle composition affinities. Meaningless ^{10}Be concentrations have
185 thus to be normalized and two proxies are currently used to retrieve the cosmogenic
186 production signal: the ^{10}Be/^{230}Th$_{xs}$ ratio [e.g. *Frank et al.*, 1997; *Christl et al.*, 2003,
187 2007, 2010; *Knudsen et al.*, 2008] and the authigenic ^{10}Be/^{9}Be ratio [*Bourlès et al.*, 1989;
188 *Henken-Mellies et al.*, 1990; *Robinson et al.*, 1995; *Carcaillet et al*., 2003, 2004a, 2004b;
189 *Leduc et al*., 2006]. Principles, as well as possible biases resulting from their use, were
190 further summarized in *Ménabréaz et al.* [2011] and references therein. In their study, the
191 authigenic ^{10}Be/^{9}Be methodology -confirmed for the first time by a ^{10}Be/^{230}Th$_{xs}$ cross-
192 evaluation conducted on the same homogenized samples- has proven to reliably correct
193 for ocean secondary contributions.

194

195 3.2 Beryllium isotopes sampling strategy determined from preliminary paleomagnetic
196 results

197 A detailed paleomagnetic study will be presented in a future paper dedicated to a
198 set of several cores collected in the same area. This paper limits itself to the relative

paleointensity curve that has been the basis for Be sampling. Natural and artificial remanent magnetizations were measured on U-Channels using a 2G cryogenic magnetometer 760 SRM model coupled with an in-line Alternating Field (AF) demagnetizer. The Natural Remanent Magnetization (NRM) and Anhysteretic Remanent Magnetization (ARM) were measured after AF steps from 5 to 60 mT. After demagnetization at 30 mT, the NRM intensity /ARM intensity ratios were taken as the best proxy for the Relative PaleoIntensity (RPI) (Figure 2B). The major feature of this preliminary RPI record consists in a deep minimum located at 7.8 m expressing the occurrence of a geomagnetic dipole low (GDL).

The ^{10}Be sampling strategy was driven by the position of this GDL. The MD05-2920 sequence was sampled every 30 cm from 4.67 to 9.67 m, and every 10 cm between 6.27 and 8.67 m.

3.3 Sample preparation and Be isotopes extraction:

The 34 selected samples were dried and crushed in an agate mortar. Of the resulting homogenized powder, ~1g was leached using a 0.04M hydroxylamine (NH_2OH-HCl) in a 25% acetic acid leaching solution [*Bourlès et al.*, 1989]. This procedure avoid the leaching of detrital Be that would strongly bias the authigenic ^{10}Be/^{9}Be ratio through detrital ^{9}Be contamination.

The resulting leaching solution was then split into two aliquots: one 2ml aliquot was separated for natural ^{9}Be measurements using Flameless Atomic Adsorption Spectrophotometry, and the remaining solution was spiked using 300 µl of a 10^{-3} g/g ^{9}Be-

carrier solution (Sharlau®) before undergoing the chemical extraction procedure summarized below. Beryllium in the leachates was first chelated at pH 7 by acetylacetone. The obtained Be-acetylacetonates were then separated using an organic solvent extraction and decomposed in acid. Beryllium oxy-hydroxydes were finally precipitated at pH 8 before being oxidized to BeO at 800°C to perform AMS (Accelerator Mass Spectrometry) measurements [*Bourlès et al.*, 1989].

3.4 Measurements:

^{10}Be concentrations were measured using the new French AMS national facility "ASTER", operating at 5MV (CEREGE). ^{10}Be concentrations were calculated from the measured spiked ^{10}Be/^{9}Be ratios (see equation given by *Ménabréaz et al.* [2011]) normalized to the NIST 4325 international standard (^{10}Be/^{9}Be = 2.79 x 10^{-11} [*Nishiizumi et al.*, 2007]). Final ^{10}Be concentrations were all corrected for ^{10}Be radioactive decay using the half-life determined by *Chmeleff et al.* [2010] and *Korschinek et al.* [2010]. Uncertainties in the measured ^{10}Be/^{9}Be ratios and in the calculated ^{10}Be concentrations may result from counting statistics and instrumental error propagation [*Arnold et al.*, 2010], according to the standard propagation of uncertainties equation [e.g. *Taylor*, 1997]. Chemistry blank ratios range from 7.66 10^{-15} to 1.39 10^{-14} and are at least 1000 times lower than the sample ratios. Measured ratios and their uncertainties are presented in Table 1.

Natural ^{9}Be concentrations were measured using a graphite-furnace atomic absorption spectrophotometer equipped with a Zeeman effect background correction

(Thermo Scientific ICE 3400 installed at the CEREGE). The absorbance of each sample was repeatedly measured at incremental steps of standard addition. The analytical precision of final ^{9}Be concentrations was determined from the reproducibility of standard addition absorptions and the fit of standard addition lines, and ranges from 0.2% to 4.6% (see Table 1).

4. The authigenic ^{10}Be/^{9}Be record

Authigenic ^{10}Be concentrations vary from 9.56 x 10^{-15} g/g to 2.44 x 10^{-14} g/g and authigenic ^{9}Be concentrations vary from 1.79 x 10^{-7} g/g to 2.60 x 10^{-7} g/g, resulting in ^{10}Be/^{9}Be ratios that range from 4.57 x 10^{-8} to 1.20 x 10^{-7}. Sample concentration and ratio values are listed in Table 1. The ^{10}Be concentration profile shows a unique major enhancement reaching a peak at 767 cm which persists along the authigenic ^{10}Be/^{9}Be ratio profile (Figure 2A) in the form of ~1.7-fold increase of the ^{10}Be/^{9}Be ratio when compared to the average value calculated over the time interval spanned by this record (7.07 x 10^{-8}). This principal enhancement is recorded between ~737 cm and ~817 cm. The rest of the profile exhibits reduced variability, with slightly lower values before than after this major increase.

The RPI record, proxy of the geomagnetic dipole moment variation, and the authigenic ^{10}Be/^{9}Be ratio, proxy of the cosmogenic nuclide production, are inversely correlated (Figure 2). The main RPI low, located between ~850 cm and ~750 cm, and the main authigenic ^{10}Be/^{9}Be ratio enhancement, located between ~737 and ~817 cm, overlap

to a large extent. The RPI minimum leads the authigenic $^{10}Be/^{9}Be$ ratio maximum by ~15 cm

Despite this slight delay which is coherent with the principle of the post-depositional magnetization lock-in depth, the two paleomagnetic and geochemical signatures must be interpreted as expressions of the same geomagnetic dipole low (GDL).

5. Age Model

The age model of core MD05-2920 is based on ten ^{14}C datings performed on the planktonic foraminifera *Globigerinoides ruber* (white), and on the correlation between the benthic $\delta^{18}O$ record and the reference benthic stack published by *Lisieki and Raymo* [2005] [Figure 3 in *Tachikawa et al.*, 2011]. After correction of the local reservoir age of 420 ± 60 yrs [*Mc Gregor et al.*, 2008], conventional ^{14}C ages were calibrated using the IntCal09 calibration set [*Reimer et al.*, 2009] and the Calib 6.1.0 software (http://intcal.qub.ac.uk/calib/)). The chronological reconstruction is presented in Figure 3C. Corresponding data can be found in Table 2. From these data, the sedimentation rates range between 12.3 and 16 cm/ka along the studied part of the MD05-2920 sequence.

6. Discussion

The authigenic $^{10}Be/^{9}Be$ record is plotted on its time scale in Figure 4a. The $^{10}Be/^{9}Be$ ratio peak can be seen recorded at ~40.8 ka, which allows its attribution to the Laschamp-related cosmogenic nuclide production enhancement in the atmosphere (see details on the chronology of the Laschamp event discussed by *Ménabréaz et al.* [2011]).

285

286 6.1 Comparison with the Laschamp ^{10}Be atmospheric overproduction records at mid and
287 high latitudes.

288 The age of the authigenic ^{10}Be/^{9}Be maximum value at ~40.8 ka remarkably
289 coincides (within uncertainties) with the age of the authigenic ^{10}Be/^{9}Be peak
290 documenting the Laschamp-related GDL recorded at ~41 ka in Portuguese Margin
291 sediment cores ([*Ménabréaz et al.*, 2011]; Figure 4b). Despite very different depositional
292 settings, these authigenic ^{10}Be/^{9}Be records are in good overall correspondence over the
293 whole studied time period. During the Laschamp GDL, the presented data indicate that
294 the ^{10}Be production was enhanced by a factor of ~1.7 at that equatorial site (enhancement
295 factors are determined from the average value over the time interval spanned by the
296 records). This agrees, within respective uncertainties, with the ~1.9-fold increase
297 measured in the authigenic ^{10}Be/^{9}Be ratio record of the Portuguese Margin [*Ménabréaz et*
298 *al.*, 2011], and also with the ~1.7-fold increase previously reported by *Carcaillet et al.*
299 [2004b] from a neighbouring core (Figure 4b). Such enhancement factors are also
300 compatible with the near-doubling of the global (i.e. latitude integrated) ^{10}Be production
301 during GDL, expected from the physically constrained algorithm [*Elsasser et al.*, 1956;
302 *Lal*, 1988] and from numerical simulations [*Masarik and Beer*, 2009] describing the
303 relation between geomagnetic moment and cosmogenic nuclides global production.
304

305 Furthermore, these sedimentary records of the ^{10}Be atmospheric overproduction
306 linked to the Laschamp GDL are concomitant with the ^{10}Be-flux peak recorded in the

307 Greenland ice cap at Summit (Figure 4) [*Muscheler et al.,* 2005], dated at ~41 ka based
308 on ice laminae counting (GICC05 timescale of the *NGRIP-dating group* [2006] and
309 references therein]. This emphasises the simultaneity of the Laschamp ^{10}Be
310 overproduction records in paleoclimatic archives at very different locations. Over the
311 entire studied time interval, the presented authigenic ^{10}Be/^{9}Be records are remarkably
312 similar both in time and in amplitude with the Greenland ^{10}Be-flux. This coherency of the
313 signals observed for different archives located at different latitudes and in such various
314 climatic and environmental conditions most likely allows ruling out the hypothesis that
315 variability in ^{10}Be/^{9}Be ratios in core MD05-2920 arises primarily from changes in the
316 continental runoff and oceanic regimes.

317 In addition to validating the pertinence of the authigenic ^{9}Be normalization to
318 account for secondary effects, these observations more importantly demonstrate that the
319 ^{10}Be production signal in marine sediments is a global signal because of the lack of any
320 significant latitude effects. This remarkable correspondence also confirms that the
321 Greenland ^{10}Be-flux signal over long time-scales is dominantly modulated by the
322 geomagnetic dipole moment [e.g. *Muscheler et al.,* 2005], implying that a significant part
323 of the ^{10}Be deposited in Greenland ice has been homogenized in the atmosphere. This
324 supports a ^{10}Be residence time of several years in the atmosphere [*Baroni et al.,* 2011].

325

326 6.2 A marine stacked record of the ^{10}Be production rates.

327 The authigenic ^{10}Be/^{9}Be records obtained from sedimentary sequences from two
328 different regions -West Equatorial Pacific (MD05-2920) and Northeast Atlantic (MD95-

329 2042 and MD04-2811 cores)- are normalized to their own average value and plotted on
330 their own chronologies in Figure 5 (MD05-2920 chronological data are presented in
331 Section 5 and Table 2; MD95-2042 and MD04-2811 chronological data are presented in
332 *Ménabréaz et al.* [2011]).

333 These records are compared to the Greenland ^{10}Be flux (GRIP and GISP2 ice
334 cores), normalized to its own average value and plotted in Figure 5 on its own chronology
335 as established by multiparameter counting of annual layers [*Andersen et al.*, 2006;
336 *NGRIP-dating group*, 2006; *Rasmussen et al.*, 2006]. The glacial part of this time scale
337 has an estimated associated error of 2% back to 40 ka and of 5–10% back to 57 ka. The
338 correspondence is remarkable despite noise and distortion introduced by 1) analytical
339 uncertainties, 2) chronological uncertainties (e.g. linear interpolation between ~37 ka and
340 62 ka in the MD05-2920 core), and 3) recording processes (e.g. changes in sediment
341 accumulation rate and/or sediment properties). A composite record of the normalized
342 authigenic ^{10}Be/^{9}Be ratios is thus constructed and arithmetically averaged using a 1000-
343 year sliding window offset by 500 years. Associated uncertainties (1σ) are standard
344 deviations around computed average values.

345 The normalized authigenic ^{10}Be/^{9}Be stack (Figure 6; Table 3) indicates that the
346 global 1000-year averaged ^{10}Be production rate increased by a factor of ~1.5 at ~41 ka
347 (age of the Laschamp GDL) compared to the long-term average calculated over the 20-50
348 ka. No other significant enhancement of ^{10}Be production is evidenced over the studied
349 time interval.

The comparison of the normalized authigenic $^{10}Be/^{9}Be$ stack with the Greenland ice sheet ^{10}Be-record (smoothed over a 1000-year window and plotted on its own timescale) evidences a remarkable similarity (Figure 6). This is especially noticeable considering that both records are obtained using very different techniques and recording archives. For the first time, the Greenland ^{10}Be deposition millennial-scale flux variations can be compared with an authigenic $^{10}Be/^{9}Be$ reference record composed by low and mid latitudes records. Their similarity confirms that the modulation mechanism is common and that they constitute proxies of the global atmospheric ^{10}Be production. Since there is no geomagnetic modulation of the cosmogenic nuclides production at high latitudes, the similarity of these ^{10}Be production records confirms that the major part of the ^{10}Be deposited in Greenland ice is transported from lower latitudes through atmospheric homogenization [e.g. *Muscheler et al.,* 2005; *Heikkilä et al.,* 2008]. The observed agreement of the Greenland ice record with oceanic sediment records located in high particle flux areas (where ^{10}Be residence time with respect to scavenging is ~500 yrs [*Anderson et al.,* 1990; *Ku et al.,* 1990]) also suggests that both signal attenuation and time lags potentially resulting from an oceanic ^{10}Be reservoir effect are minimized. Indeed, such settings reduce the ^{10}Be residence time in the water column and the effects of surface sediment mixing by the burrowing fauna.

6.3. Construction of a ^{10}Be-derived virtual dipole moment record

The normalized authigenic $^{10}Be/^{9}Be$ stack is then used to reconstruct the modulating dipole moment variation. Normalized $^{10}Be/^{9}Be$ values are calibrated using

absolute VDM values determined from absolute paleointensities measured on lava flows and drawn from the literature. For coherency, the same absolute VDM values as in *Ménabréaz et al.* [2011] are taken from the GEOMAGIA-50 database, because they are assumed to be representative of the VDM values over the 20-50 ka time period. Since ^{10}Be production rates are inversely proportional to VDM values [*Elsasser et al.*, 1956; *Lal*, 1988], (1) the normalized ^{10}Be/^{9}Be maximum value (i.e. [1.52 ± 0.26] x 10^{-8}) was assigned to the minimum VDM value linked to the LE (i.e. 1.06 ± 0.05 x 10^{22} A.m^2 [*Levi et al.*, 1990]), (2) the average of the normalized ^{10}Be/^{9}Be values lower than 0.78 (mean – 1 sigma) was assigned to the average of the VDM values higher than 8.70 A.m^2 (mean + 1 sigma), and (3) the average of the normalized ^{10}Be/^{9}Be values comprised between 0.78 and 1.12 ([mean ± 1 sigma] interval) was assigned to the average of the VDM values comprised between 3.62 and 8.70 A.m^2 ([mean ± 1 sigma] interval). This empirical polynomial fit obtained using the absolute VDM values is compared to the curve derived from Elsasser's algorithm, obtained using relative VDM values (as noted by *Lal*, [1992]) and applied to the normalized ^{10}Be production values derived from this study: their similarity reinforces the validity of the proposed calibration procedure (Figure 7). The polynomial fit between ^{10}Be and absolute VDM data is then applied to the whole ^{10}Be dataset. The ^{10}Be-derived absolute VDM reconstruction is shown in Figure 8 (data are listed in Table 3).

The ^{10}Be-derived absolute VDM reconstruction is compared to the reference relative paleointensity stacks, evidencing an overall good agreement with the GLOPIS-75 curve [*Laj et al.*, 2004], particularly between 36 and 51 ka (Figure 8). A major difference appears at 30-33 ka, where high RPI values in GLOPIS follow the reduction generally

attributed to the Mono Lake excursion. The ^{10}Be-derived VDM record only shows a small amplitude reduction at ~34 ka followed by a progressive increase until ~22 ka, interrupted by another transient reduction at ~26 ka. The ^{10}Be-derived VDM record presents similar averaged values to the SINT 800 stack but points out a larger amplitude and narrower VDM reduction at the Laschamp age, due to the SINT-800 smoothing which results from stacking numerous records.

6.4 Geomagnetic implications

These cosmogenic nuclide production records and their translation as VDM records contribute to the understanding of the relation between the ^{10}Be production rates and the dipole moment values, and to the timing and quantification of the VDM reduction accompanying the geomagnetic excursions documented in the studied time interval. Indeed, the trends of the ^{10}Be-derived VDM stack result from the construction of robust chronologies along the two studied sedimentary sequences and are further supported by the tight correlation between the sedimentary and ice cores ^{10}Be production records. Estimates of durations and rates of changes are thus enabled.

While paleomagnetic sedimentary records rarely provide precise estimations of the duration of excursions due to 1) imperfect remanent magnetization acquisition in low intensity field, 2) remagnetization after recovery of higher intensity field [e.g. *Coe and Liddicoat,* 1994; *Roberts and Winklhofer,* 2004], and 3) latitudinal and longitudinal dependency of the geomagnetic vector variation, the ^{10}Be production records provide a global perspective on the timing and amplitude of the VDM variation.

The Laschamp Excursion

The global cosmogenic ^{10}Be enhancement at the time of the Laschamp excursion (~41 ka) recorded in the marine reference $^{10}Be/^{9}Be$ record is fully concordant with that reported from ^{10}Be deposition rates in the Greenland ice cores: when the dipole field vanishes (VDM ~$1x10^{22}$ $A.m^2$), the 1 ka average global ^{10}Be production rate is multiplied by ~1.5, while individual unsmoothed records report a 1.7- to 1.9- fold increase of the ^{10}Be production.

The duration of the enhancement phase can be estimated using, either the ^{10}Be value above "mean+1σ" which provides a maximum duration of 2500 years, or above "mean + 2σ", which provides a maximum duration of 1500 years. This provides the same estimated duration of VDM loss as that deduced from ice core records [*Wagner et al.*, 2000b; *Muscheler et al*., 2005] and from the GLOPIS-75 stack [*Laj et al.*, 2004].

The VDM collapse from ~11 x 10^{22} $A.m^2$ to ~1 x 10^{22} $A.m^2$ occurred between 48 and 41 ka, yielding an average pre-excursional VDM loss rate of ~ -1.4 x 10^{22} $A.m^2.ka^{-1}$. The main VDM loss occurred after 44 ka with a loss rate of ~ -1.5 x 10^{22} $A.m^2.ka^{-1}$. It is interesting to note that from archeomagnetic reconstructions [*Gallet et al.*, 2009], the computed VDM loss rate of ~ -2.7 x 10^{22} $A.m^2$ over the last millennium appears significantly higher than the Laschamp pre-excursional rates.

The Mono Lake Excursion

437 The ^{10}Be production reference records do not evidence any global significant
438 increase in the atmospheric production of cosmogenic nuclides at the age of the Mono
439 Lake excursion (~34 ka). The corresponding VDM value (4 x 10^{22} A.m^2) obtained from
440 our reconstruction (Figure 8) is consistent with those determined from absolute
441 paleointensities measured on lava flows (though it must be stressed that VDM values
442 computed from low paleointensity data are, by definition, biased by non-dipole field
443 contributions). In Hawaii, 9 of the 11 lavas recording the excursion yield VADM
444 estimates of ~4 x 10^{22} A.m^2 [*Laj et al.*, 2002; *Teanby et al.*, 2002]. In the Canary Islands,
445 the 3 studied lava flows yield VADM values of (4.3 ± 1.3), (1.6 ± 0.3), and (2.5 ± 0.8) ×
446 10^{22} Am^2 [*Kissel et al.* 2011]. Compilation of New Zealand PI data [*Mochizuki et al.*,
447 2006; *Cassidy and Hill* 2009] provides a VADM value of ~2.5 10^{22} A.m^2 [*Kissel et al.*,
448 2011].

449 The short duration of the GDL associated with the Mono Lake excursion may
450 contribute to the lack of cosmogenic nuclide overproduction signature in marine archives.
451 Taking into account a (standard) bioturbation depth of 15 cm, the related overproduction
452 may not be recorded in these sequences. However, ^{10}Be ice records, despite their high
453 resolution, do not exhibit either any overproduction signature either (see Muscheler et al.,
454 2005), contrary to the ^{36}Cl record [*Wagner et al.*, 2000a]. The different response of these
455 two cosmogenic nuclides, similarly produced through nuclear reactions induced in the
456 atmosphere by cosmic ray particles has led to questions concerning the reliability of the
457 ^{36}Cl peak [see *Delmas et al.*, 2004].

458

7. Conclusion and perspectives

The $^{10}Be/^{9}Be$ record of the MD05-2920 sediment core is the first reliable authigenic $^{10}Be/^{9}Be$ evidence of cosmogenic nuclide ^{10}Be overproduction at low latitude at the age of the Laschamp excursion (41 ka). Together with other records of marine and terrestrial archives it confirms the global synchronicity of the ^{10}Be overproduction in the atmosphere generated by the loss of the geomagnetic dipole. The compilation of authigenic $^{10}Be/^{9}Be$ marine records indicates that the global ^{10}Be production rates at 41 ka were enhanced by a ~1.5 factor compared to the average over the 20-60 ka interval. The comparison of the authigenic $^{10}Be/^{9}Be$ marine stack with the Greenland ^{10}Be flux record (smoothed by 1000-year averaging) evidences a good coherency of the timing and amplitude of ^{10}Be production at high, mid and low latitudes. This confirms that the ^{10}Be overproduction signal has a global significance, as expected from a geomagnetic dipole moment loss.

The calibration of the sedimentary $^{10}Be/^{9}Be$ stack using absolute virtual dipole moment values provides an independent tool to reconstruct geomagnetic dipole moment variations. This allows computing the loss rate leading to the Laschamp dipole minimum ($\sim -1.5 \times 10^{22}$ $A.m^2.ka^{-1}$). This constitutes an interesting criterion to assess the loss rate of the historical field.

In constrast with the relavant signatures in the GLOPIS-75 relative paleointensity stack and in absolute paleointensity data sets, the absence of significant cosmogenic response at 34 ka suggests that the Mono Lake dipole low was hardly sufficient to trigger a significant cosmogenic overproduction. This demonstrates that if the Mono lake

481 excursion really occurred at that time, the duration and amplitude of the dipole
482 weakening were very limited compared to that of the Laschamp.

483 The ^{10}Be overproduction quantified in this study constitutes a reliable basis to
484 calibrate radiocarbon production and *in situ* cosmogenic nuclides production. For
485 example, it can help to understand the atmospheric ^{14}C concentration variations recorded
486 near 41 ka and near 34 ka in delta ^{14}C series [e.g. *Hughen et al.,* 2004; *Reimer et al.*,
487 2009], which were probably produced by the Laschamp and Mono Lake geomagnetic
488 dipole lows.

489 The ^{10}Be production peak linked to the Laschamp dipole low can be used as a
490 global tie point for correlation of high-resolution paleoclimatic series obtained from high
491 quality archives.

492

493

494

495

496

497

498

499

Acknowledgements:

This work is a contribution to the MAG-ORB (ANR- 09-BLAN-0053-01) project, which is funded by the French Agence Nationale de la Recherche (ANR). We aknowledge V. Guillou for technical assistance during chemical procedures, and F. Demory for help in U-channel sampling and during paleomagnetic data acquisition. R. Muscheler kindly provided the ^{10}Be ice cores data used in this study. We also thank here M. Arnold, G. Aumaître, and K. Keddadouche for their valuable assistance during ^{10}Be measurements at the ASTER AMS national facility (CEREGE, Aix-en-Provence), which is supported by the INSU/CNRS, the French Ministry of Research and Higher Education, IRD and CEA. We acknowledge the scientific and technical crew of R.V. *Marion Dufresne* who collected core MD05-2920 during the MD148-PECTEN Cruise. We thank Prof. M. Frank and an anonymous reviewer for their helpful comments in preparing the final version of the manuscript.

Reference list:

Andersen, K.K., Svensson, A., Rasmussen, S.O., Steffensen, J.P., Johnsen, S.J., Bigler, M., Röthlisberger, R., Ruth, U., Siggaard-Andersen, M.-L., Dahl-Jensen, D., Vinther, B.M., Clausen, H.B., 2006. The Greenland Ice Core Chronology 2005, 15–42 ka. Part 1: constructing the time scale. Quat. Sci. Rev. 25, 246–257.

Anderson R.F., Y. Lao, W.S. Broecker, S.E Trumbore., H.J. Hofmann, and W. Wolfli (1990), Boundary scavenging in the Pacific Ocean: a comparison of ^{10}Be and ^{231}Pa, *Earth and Planet. Sci. Lett*. *96*, 287-304.

Arnold, M., S. Merchel, D.L. Bourlès, R. Braucher, L. Benedetti, R.C. Finkel, G. Aumaître, A. Gottdang, and M. Klein (2010), The French accelerator mass spectrometry facility ASTER: Improved performance and developments, *Nucl. Instrum. Methods Phys. Res. Sect. B 268*, 1954-1959.

Bard, E., and M. Frank, (2006), Climate change and solar variability: What's new under the sun? *Earth and Planet. Sci. Lett*. *248*, 1–14.

539 Baroni, M., E. Bard, J.R Petit, O. Magnan, and D.L Bourlès (2011), Volcanic and solar
540 activity, and atmospheric circulation influences on cosmogenic 10Be fallout at Vostok
541 and Concordia (Antarctica) over the last 60 years., *Geochim. Cosmochim. Acta, ISSN*
542 *0016-7037*, doi: 10.1016/j.gca.2011.09.002.

543 Beaufort, L., A.W. Droxler, M.-T Chen, and party, t.m.o.t.s., 2005. MD148 / IMAGES XIII,
544 PECTEN 2005 Cruise Report.

545 Beer, J., A. Blinov, G. Bonani, R.C. Finkel, H.J. Hofman, B. Lelmann, H. Oeschger, A.
546 Sigg, J. Schwander, T. Staffelbach, B. Stauffer, M. Suter, and W. Wolfli, (1990), Use of
547 ^{10}Be in polar ice to trace the 11-year cycle of solar activity, *Nature 347,* 164-166.

548 Benson, L., J. Liddicoat, J. Smoot, A Sarna-Wojcicki. R. Negrini, and S. Lund, (2003), Age
549 of the Mono Lake excursion and associated tephra, *Quat. Sci. Rev. 22*, 135-140.

550 Bonhommet, N., and J. Babkine (1967), Sur la présence d'aimantations inverses dans la
551 Chaîne des Puys — Massif Central, France, *C.R.A.S. Paris 264*, 92.

552 Bonhommet, N., and J. Zahringer (1969), Paleomagnetism and potassium argon age
553 determinations of the Laschamp geomagnetic polarity event, *Earth Planet. Sci. Lett. 6*,
554 43–46.

555 Bourlès, D., G.M. Raisbeck, and F. Yiou (1989), ^{10}Be and ^{9}Be in marine sediments and their
556 potential for dating, *Geochim. Cosmochim. Acta 53*, 443-452.

557 Carcaillet, J., N. Thouveny, and D.L. Bourlès (2003), Geomagnetic moment instability
558 between 0.6 and 1.3 Ma from cosmonuclide evidence, *Geophys. Res. Lett. 30*, 1792.

559 Carcaillet, J., D.L. Bourlès, and N. Thouveny (2004a), Geomagnetic dipole moment and
560 10Be production rate intercalibration from authigenic $^{10}Be/^{9}Be$ for the last 1.3 Ma,
561 *Geochem. Geophys. Geosyst. 5*, 397-412, Q05006, doi: 10.1029/2003GC000641.

562 Carcaillet, J., D.L. Bourlès, N. Thouveny, and M. Arnold, (2004b), A high resolution
563 authigenic $^{10}Be/^{9}Be$ record of geomagnetic moment variations over the last 300 ka from
564 sedimentary cores of the Portuguese margin, *Earth Planet. Sci. Lett. 219*, 397-412.

565 Cassata, W.S., B.S. Singer, and J. Cassidy, (2008), Laschamp and Mono Lake geomagnetic
566 excursions recorded in New Zealand, *Earth Planet. Sci. Lett. 268*, 76-88.

567 Cassidy, J., and M. J. Hill (2009), Absolute palaeointensity study of the Mono Lake
568 excursion recorded by New Zealand basalts, *Phys. Earth Planet. Inter. 172*, 225–234.

569 Channell, J. (2006), Late Brunhes polarity excursions (Mono Lake, Laschamp, Iceland
570 Basin and Pringle Falls) recorded at ODP Site 919 (Irminger Basin), *Earth Planet. Sci.*
571 *Lett. 244*, 378-393.

572 Channell, J.E.T., C. Xuan, and D.A. Hodell, (2009), Stacking paleointensity and oxygen
573 isotope data for the last 1.5 Myr (PISO-1500), *Earth Planet. Sci. Lett. 283*, 14-23.

574 Chauvin A., R.A. Duncan, N. Bonhommet, and S. Levi (1989), Paleointensity of the earth's
575 magnetic field and K–Ar dating of the Louchadière volcanic flow (central France): New
576 evidence for the Laschamp Excursion, *Geophys. Res. Lett. 16*, 1189–1192.

577 Chmeleff, J., F. von Blanckenburg, K. Kossert, and D. Jakob (2010), Determination of the
578 ^{10}Be half-life by multicollector ICP-MS and liquid scintillation counting, *Nucl. Instrum.*
579 *Methods Phys. Res. Sect. B 268*, 192-199.

580 Christl, M., C. Strobl, and A. Mangini, (2003), Beryllium-10 in deep-sea sediments: a tracer
581 for the Earth's magnetic field intensity during the last 200,000 years, *Quat. Sci. Rev. 22*,
582 725-739.

583 Christl, M., A. Mangini, and P.W. Kubik (2007), Highly resolved Beryllium-10 record from
584 ODP Site 1089--A global signal? *Earth Planet. Sci. Lett. 257*, 245-258.

585 Christl, M., J. Lippold, F. Steinhilber, F. Bernsdorff, and A. Mangini, (2010),
586 Reconstruction of global ^{10}Be production over the past 250 ka from highly
587 accumulating Atlantic drift sediments, *Quat. Sci. Rev. 29*, 2663-2672.

588 Coe, R.S., and J.C. Liddicoat (1994), Overprinting of natural magnetic remanence in lake
589 sediments by subsequent high intensity field, *Nature 367*, 57-59.

590 Condomines M. (1980), Age of the Olby-Laschamp geomagnetic polarity event, *Nature 286*,
591 697–699.

592 Cresswell, G.R. (2000), Coastal currents of northern Papua New Guinea, and the Sepik
593 River Outflow, *Mar. Freshw. Res. 51*, 553-564.

594 Denham, C.R., and A. Cox, (1971), Evidence that the Laschamp polarity event did not occur
595 13300–30400 years ago, *Earth Planet. Sci. Lett. 13*, 181-190.

596 Delmas R.J., J. Beer, H.A. Synal, R. Muscheler, J.R. Petit, and M. Pourchet (2004), Bomb-
597 test ^{36}Cl measurements in Vostok snow (Antartica) and the use of ^{36}Cl as a dating tool
598 for deep ice cores, *Tellus 56B*, 492-498.

599 Elsasser, W., E.P. Ney, and J.R. Winckler (1956), Cosmic-ray intensity and geomagnetism,
600 *Nature 178*, 1226-1227.

601 Finkel, R.C., and K. Nishiizumi (1997), Beryllium-10 concentrations in the Greenland Ice
602 Sheet Project 2 ice core from 3–40 ka, *J. Geophys. Res. 102,* 26699-26706.

603 Frank, M., B. Schwarz, S. Baumann, P.W. Kubik, M. Suter, and A. Mangini (1997), A 200
604 kyr record of cosmogenic radionuclide production rate and geomagnetic field intensity
605 from ^{10}Be in globally stacked deep-sea sédiments, *Earth Planet. Sci. Lett. 149*, 121-129.

606 Frank, M. (2000), Comparison of cosmogenic radionuclide production and geomagnetic
607 field intensity over the last 200,000 years, *Phil. Trans. R. Soc. Lond. A 358*, 1089-1107.

608 Gallet Y., A. Genevey, M. Le Goff, N. Warmé, J. Gran-Aymerich, and A. Lefèvre (2009),
609 On the use of archeology in geomagnetism and vice-versa : Recent developments in
610 archeomagnetism, *C.R Phys. 10*, 630-648.

611 Gillot, P.Y., J. Labeyrie, C. Laj, G. Valladas, G. Guerin, G. Poupeau, and G. Delibrias
612 (1979), Age of the Laschamp geomagnetic polarity excursion revisited, *Earth Planet.*
613 *Sci. Lett. 42*, 444–450.

614 Guillou, H., B.S. Singer, C. Laj, C. Kissel, S. Scaillet, and B.R. Jicha (2004), On the age of
615 the Laschamp geomagnetic excursion, *Earth Planet. Sci. Lett. 227*, 331-343.

616 Guyodo, Y., and J.P. Valet (1999), Global changes in intensity of the Earth's magnetic field
617 during the past 800 kyr, *Nature 399*, 249-252.

618 Hall, C.M., and D. York (1978), K–Ar and ^{40}Ar/^{39}Ar age of the Laschamp geomagnetic
619 polarity reversal, *Nature 274*, 462–464.

620 Hanna, R. L., and K. L. Verosub (1989), A review of lacustrine paleomagnetic records from
621 Western North America : 0-40000 years BP, *Phys. Earth Planet. Inter. 56*, 76-95.

622 Heikkilä, U., J. Beer, and J. Feichter (2008), Meridional transport and deposition of
623 atmospheric ^{10}Be, *Atmos. Chem. Phys. Discuss., 8*, 16819–16849, 2008 www.atmos-
624 chem-phys-discuss.net/8/16819/2008/

625 Heikkilä, U., J. Beer, J.A. Abreu, and F. Steinhilber (2011), On the Atmospheric Transport
626 and Deposition of the Cosmogenic Radionuclides (^{10}Be): A Review, *Space Sci. Rev.*,
627 doi: 10.1007/s11214-011-9838-0.

628 Henken-Mellies, W.U., J. Beer, F. Heller, K.J. Hsü¸ C. Shen, G. Bonani, H.J. Hofmann, M.
629 Suter, and W. Wölfli (1990), ^{10}Be and ^{9}Be in South Atlantic DSDP Site 519: Relation to
630 geomagnetic reversals and to sediment composition, *Earth Planet. Sci. Lett. 98*, 267-
631 276.

632 Hughen, K., S. Lehman, J. Southon, J. Overpeck, O. Marchal, C. Herring, and J. Turnbull
633 (2004), ^{14}C Activity and Global Carbon Cycle Changes over the Past 50,000 Years,
634 *Science 303*, 202-207.

635 Kawahata, H., A. Suzuki, and H. Ohta (2000), Export fluxes in the Western Pacific Warm
636 Pool, *Deep-Sea Res.I 47*, 2061-2091.

637 Kent, D.V., S.R. Hemming, and B.D. Turrin (2002), Laschamp Excursion at Mono Lake?
638 *Earth Planet. Sci. Lett. 197*, 151-164.

639 Kineke, G.C., K.J. Woolfe, S.A. Kuehl, J.D. Milliman, T.M. Dellapenna, and R.G. Purdon
640 (2000), Sediment export from the Sepik River, Papua New Guinea: evidence for a
641 divergent sediment plume, *Cont. Shelf Res. 20*, 2239-2266.

642 Kissel, C., H. Guillou, C. Laj, J.C. Carracedo, S. Nomade, F. Perez-Torrado, and C.
643 Wandres (2011), The Mono Lake excursion recorded in phonolitic lavas from Tenerife
644 (Canary Islands): paleomagnetic analyses and coupled K/Ar and Ar/Ar dating, *Phys.*
645 *Earth Planet. Inter. 187*, 232-244.

646 Knudsen, M.F., G.M. Henderson, M. Frank, C. Mac Niocaill, and P.W. Kubik (2008), In-
647 phase anomalies in Beryllium-10 production and palaeomagnetic field behaviour during
648 the Iceland Basin geomagnetic excursion, *Earth Planet. Sci. Lett. 265*, 588-599.

649 Korhonen, K., F. Donadini, P. Riisager, and L.Pesonen (2008), GEOMAGIA50: an
650 archeointensity database with PHP and MySQL, *Geochem. Geophys. Geosyst. 9 (4)*,
651 Q04029, doi: 10.1029/2007GC001893.

652 Korschinek, G., A. Bergmaier, T. Faestermann, U.C. Gerstmann, K. Knie, G. Rugel, A.
653 Wallner, I. Dillmann, G. Dollinger, C.L. von Gostomski, K. Kossert, M. Maiti, M.
654 Poutivtsev, and A. Remmert (2010), A new value for the half-life of ^{10}Be by Heavy-Ion
655 Elastic Recoil Detection and liquid scintillation counting, *Nucl. Instr. Meth. in Phys.*
656 *Res. Sect. B 268*, 187-191.

657 Kristjansson, L., and A.A. Gudmundsson, (1980), Geomagnetic excursions in late-glacial
658 basalt outcrop in south-western Iceland, *Geophys. Res. Lett. 7*, 337–340.

659 Ku, T.L., M. Kusakabe, C.I. Measures, J.R., Southon, G. Cusimano, J.S. Vogel, D.E.
660 Nelson, and S. Nakaya (1990), Beryllium isotope distribution in the western North
661 Atlantic : a comparison to the Pacific, *Deep-Sea Res. 37*, 795-808.

662 Laj, C., C. Kissel, A. Mazaud, J.E.T. Channell, and J. Beer (2000), North Atlantic
663 paleointensity stack since 75 ka (NAPIS-75) and the duration of the Laschamp event,
664 *Philos. Trans. R. Soc. Lond. 358*, 1009–1025.

665 Laj, C., C. Kissel, V. Scao, J. Beer, D.M. Thomas, H. Guillou, R. Muscheler, and G. Wagner
666 (2002), Geomagnetic intensity and inclination variations at Hawaii for the past 98 kyr
667 from core SOH-4 (Big Island): a new study and a comparison with existing
668 contemporary data, *Phys. Earth Planet. Inter. 129*, 205–243.

669 Laj, C., C. Kissel, and J. Beer (2004), High resolution global paleointensity stack since 75
670 kyr (GLOPIS-75) calibrated to absolute values, In: Channell, J.E.T., D.V. Kent, W.
671 Lowrie, and J.G. Meert, (Eds.), Timescales of the Paleomagnetic Field, *Geophys.*
672 *Monogr. 145*.

673 Lal, D. (1988), Theoretically expected variations in the terrestrial cosmic-ray production
674 rates of isotopes, *Soc. Italia. di Fisica-Bologna-Italy XCV corso*, 216-233.

675 Lal, D. (1992), Expected secular variations in the global terrestrial production rate of
676 radiocarbon, In: Bard, E., and W.S. Broecker (Eds.), The Last Deglaciation: Absolute
677 and Radiocarbon Chronologies, Series I, *Global Environmental Change 2*, 114–126.

678 Lal, D., and B. Peters (1967), Cosmic ray produced radioactivity on the Earth, in: Flugge, S.
679 (Ed.), *Handb. Phys. Springer*, pp. 551-612.

680 Leduc, G., N. Thouveny, D.L Bourlès, C.L. Blanchet, and J.T Carcaillet (2006), Authigenic
681 $^{10}Be/^{9}Be$ signature of the Laschamp excursion: A tool for global synchronisation of
682 paleoclimatic archives, *Earth Planet. Sci. Lett. 245*, 19-28.

683 Levi, S., H. Gudmunsson, R.A. Duncan, L. Kristjansson, P.V Gillot, and S.P. Jacobsson
684 (1990), Late Pleistocene geomagnetic excursion in Icelandic lavas: Confirmation of the
685 Laschamp excursion, *Earth Planet. Sci. Lett. 96*, 443–457.

686 Liddicoat, J.C. (1992), Mono Lake Excursion in Mono Basin, California, and at Carson Sink
687 and Pyramid Lake, Nevada, *Geophys. J. Intern. 108*, 442-452.

688 Lisiecki, L.E. and M.E. Raymo (2005), A Pliocene-Pleistocene stack of 57 globally
689 distributed benthic $\delta^{18}O$ record, *Paleoceanography*, *20*, 1-17,
690 doi:10.1029/2004PA001071

691 Lund, S.P., M. Schwartz, L. Keigwin, and T. Johnson (2005), Deep-sea sediment records of
692 the Laschamp geomagnetic field excursion (<41,000 calendar years before present), *J.*
693 *Geophys. Res. 110*, Q12006.

694 Lund, S.P., J.S. Stoner, J.E.T. Channell, and G. Acton (2006), A summary of Brunhes
695 paleomagnetic field variability recorded in ODP Cores, *Phys. Earth Planet. Int. 156*,
696 194–204.

697 Masarik, J., and J. Beer (1999), Simulation of particle fluxes and cosmogenic nuclide
698 production in the Earth's atmosphere, *J. Geophys. Res. 104*, 12099-12111.

699 Masarik, J., and J. Beer (2009), An updated simulation of particle fluxes and cosmogenic
700 nuclide production in the Earth's atmosphere. *J. Geophys. Res. 114*, D1110,
701 doi:10.1029/2008JD010557.

McGregor, H.V., M.K. Gagan, M.T. McCulloch, E. Hodge, and G. Mortimer (2008), Mid-Holocene variability in the marine ^{14}C reservoir age for northern coastal Papua New Guinea, *Quat. Geochronol. 3*, 213-225.

Ménabréaz, L., N. Thouveny, D. L Bourlès, P. Deschamps, B. Hamelin, and F. Demory (2011), The Laschamp geomagnetic dipole low expressed as a cosmogenic ^{10}Be atmospheric overproduction at ~41 ka, *Earth Planet. Sci. Lett. 312*, 305-317.

Milliman, J.D., K.L. Farnsworth, and C.S. Albertin (1999), Flux and fate of fluvial sediments leaving large islands in the East Indies, *J. Sea Res. 41*, 97-107.

Mochizuki, N., H. Tsunakawa, H. Shibuya, T. Tagami, A. Ozawa, J. Cassidy, and I.E.M. Smith (2004), K–Ar ages of the Auckland geomagnetic excursions, *Earth Planets Space 56*, 283–288.

Mochizuki, N., H.Tsunakawa, H. Shibuya, J. Cassidy, and I.E.M. Smith (2006), Paleointensities of the Auckland geomagnetic excursions, *Phys. Earth Planet. Inter. 154*, 168–179.

Mochizuki, N., H.Tsunakawa, H. Shibuya, T. Tagami, A. Ozawa, and I.E.M. Smith (2007), Further K–Ar dating and paleomagnetic study of the Auckland geomagnetic excursions, *Earth Planets Space 59*, 755–761.

Muscheler, R., J. Beer, P.W. Kubik, and H.A. Synal (2005), Geomagnetic field intensity during the last 60,000 years based on ^{10}Be and ^{36}Cl from the Summit ice cores and ^{14}C. *Quat. Sci. Rev. 24*, 1849-1860.

722 Negrini, R.M., J.O Davis, and K.L. Verosub (1984), Mono Lake geomagnetic excursion
723 found at Summer Lake, Oregon, *Geology 12*, 643-646.

724 Negrini, R., K.F Erbes, A.M. Herrera, A.P Roberts, A. Cohen, M. Palacios-Fest, P.E.
725 Wigand, and F. Foit (2000), A paleoclimate record for the past 250,000 years from
726 Summer Lake, Oregon, USA: I. Age control and magnetic lake level proxies, *J.*
727 *Paleolimn. 24*, 125-149.

728 Nishiizumi, K., M. Imamura, M.W. Caffee, J.R. Southon, R.C. Finkel, and J. McAninch
729 (2007), Absolute calibration of 10Be AMS standards, *Nucl. Instr. Meth. in Phys. Res.*
730 *Sect. B 258*, 403-413.

731 NGRIP-dating-group (2006), Greenland Ice Core Chronology 2005 (GICC05), IGBP
732 PAGES/World Data Center for Paleoclimatology Data Contribution Series # 2006-118.
733 NOAA/NCDC Paleoclimatology Program, Boulder CO, USA.

734 Nowaczyk, N.R., and J. Knies (2000), Magnetostratigraphic results from the eastern Arctic
735 ocean: AMS ^{14}C ages and relative paleointensity data of the mono lake and Laschamp
736 geomagnetic reversal excursions, *Geophys. J. Intern. 140*, 185-197.

737 Plenier, G., J.P. Valet, G. Guérin, J.C Lefêvre, M. LeGoff, and B. Carter-Stiglitz (2007),
738 Origin and age of the directions recorded during the Laschamp event in the Chaîne des
739 Puys (France), *Earth Planet. Sci. Lett. 259*, 414-431.

740 Raisbeck, G.M., F. Yiou, M. Fruneau, J.M Loiseaux, M. Lieuvin, and J.C. Ravel (1981),
741 Cosmogenic Be-10/Be-7 as a probe of atmospheric transport processes, G*eophys. Res.*
742 *Lett. 8*, 1015-1018.

743 Raisbeck, G. M., F. Yiou, J. Jouzel, J.R Petit, E. Bard, and N. I Barkov (1992), ^{10}Be
744 deposition at Vostok, Antarctica, during the last 50000 years and its relationship to
745 possible cosmogenic production variations during this period, in: Bard, E., and W.S.
746 Broecker (Eds.), The Last Deglaciation: Absolute and Radiocarbon Chronologies,
747 Series I, *Global Environmental Change 2*, 127–139.

748 Rasmussen, S.O., Seierstad, I.K., Andersen, K.K., Bigler, M., Dahl-Jensen, D., Johnsen,
749 S.J., 2006. NGRIP, GRIP, and GISP2 Synchronization Match Points. IGBP
750 PAGES/World Data Center for Paleoclimatology. Data Contribution Series # 2006-120.
751 NOAA/NCDC Paleoclimatology Program, Boulder CO, USA.

752 Reimer, P.J., M.G.L. Baillie, E. Bard, A. Bayliss, J.W Beck, P.G. Blackwell, C. Bronk
753 Ramsey, C.E. Buck, G.S. Burr, R.L. Edwards, M. Friedrich, P.M. Grootes, T.P
754 Guilderson, I. Hajdas, T.J. Heaton, A.G Hogg, K.A. Hughen, K.F. Kaiser, B. Kromer,
755 G. McCormac, S. Manning, R.W Reimer, D.A. Richards, J.R. Southon, S. Talamo,
756 C.S.M. Turney, J. van der Plicht, and C.E Weyhenmeyer (2009), IntCal09 and
757 Marine09 radiocarbon age calibration curves, 0-50000 Years cal BP, *Radiocarbon 51*,
758 1111-1150.

759 Roberts, A.P., and M. Winklhoferb (2004), Why are geomagnetic excursions not always
760 recorded in sediments? Constraints from post-depositional remanent magnetization
761 lock-in modelling, *Earth Planet. Sci. Lett. 227*, 345-359.

762 Robinson, C., G.M Raisbeck, F. Yiou, B. Lehman, and C. Laj (1995), The relationship
763 between ^{10}Be and geomagnetic field strength records in central North Atlantic
764 sediments during the last 80 ka, *Earth Planet. Sci. Lett. 136*, 551-557.

765 Roperch, P., N. Bonhommet, and S. Levi (1988), Paleointensity of the earth's magnetic field
766 during the Laschamp excursion and its geomagnetic implications, *Earth Planet. Sci.*
767 *Lett. 8*8, 209–219.

768 Shibuya, H., J. Cassidy, I.E.M. Smith, and T. Itaya (1992), A geomagnetic excursion in the
769 Brunhes epoch recorded in New Zealand basalts, *Earth Planet. Sci. Lett. 111*, 41–48.

770 Singer, B.S., H. Guillou, B.R Jicha, C. Laj, C. Kissel, B.L Beard, and C.M. Johnson (2009),
771 $^{40}Ar/^{39}Ar$, K-Ar and ^{230}Th-^{238}U dating of the Laschamp Excursion: A radioisotopic tie-
772 point for ice core and climate chronologies, *Earth Planet. Sci. Lett. 286*, 80-88.

773 Tachikawa, K., O. Cartapanis, L. Vidal, L. Beaufort, T. Barlyaeva, and E. Bard (2011), The
774 precession phase of hydrological variability in the Western Pacific Warm Pool during
775 the past 400 ka, *Quat. Sc. Rev. 30*, 3716-3727

776 Taylor, J.R. (1997), An Introduction to Error Analysis. The study of Uncertainties in
777 Physical Measurements, *Second ed., University Science Books, Sausalito, USA.*

778 Teanby, N., C. Laj, D. Gubbins, and M. Pringle (2002), A detailed palaeointensity and
779 Inclination record from drill core SOH1 on Hawaii, *Physics Earth Planet. Inter. 131*,
780 101-140.

781 Thouveny, N., and K.M. Creer (1992), On the brievity of the Laschamp Excursion, *Bull.*
782 *Soc. Géol. Fr. 6*, 771–780.

783 Thouveny, N., J. Carcaillet, E. Moreno, G. Leduc, and D. Nérini (2004), Geomagnetic
784 moment variation and paleomagnetic excursions since 400 kyr BP: a stacked record

785 from sedimentary sequences of the Portuguese margin, *Earth Planet. Sci. Lett. 219*,
786 377-396.

787 Vlag, P., N. Thouveny, D. Williamson, P. Rochette, and F. Ben-Atig (1996), Evidence for a
788 geomagnetic excursion recorded in the sediments of Lac St. Front, France: a link with
789 the Laschamp Excursion? *J. Geophys. Res. 101*, 28211–28230.

790 Wagner, G., J. Beer, C., Laj, C. Kissel, J. Masarik, R. Muscheler, and H.A. Synal (2000a),
791 Chlorine-36 evidence for the Mono Lake event in the Summit GRIP ice core, *Earth*
792 *Planet. Sci. Lett. 181*, 1-6.

793 Wagner, G., J. Masarik, J. Beer, S. Baumgartner, D. Imboden, P.W Kubik, H.A Synal, and
794 M. Suter (2000b), Reconstruction of the geomagnetic field between 20 and 60 kyr BP
795 from cosmogenic radionuclides in the GRIP ice core, *Nucl. Instrum. Methods Phys. Res.*
796 *Sect. B 172*, 597-604.

797 Wang, B., S.C. Clemens, and P. Liu (2003), Contrasting the Indian and East Asian
798 monsoons: implications on geologic timescales, *Mar. Geol. 201*: 5-21.

799 Wang, Y.J., H. Cheng, R.L. Edwards, Z.S An, J.Y. Wu, C.C. Shen, and J.A. Dorale (2001),
800 A High-Resolution Absolute-Dated Late Pleistocene Monsoon Record from Hulu Cave,
801 China, *Science 294*, 2345-2348.

802 Webster, P.J., V.O Magana, T.N. Palmer, J. Shukla, R.A. Tomas, M. Yanai, and T.
803 Yasunari (1998), Monsoon: Processes, predictability, and prospects for prediction, *J.*
804 *Geophys. Res. 103(C7)*, 14451-14,10.

Yiou, F., G.M. Raisbeck, S. Baumgartner, J. Beer, C. Hammer, S. Johnsen, J. Jouzel, P.W. Kubik, J. Lestringuez, M. Stiévenard, M. Sutter, and P. Yiou (1997), Beryllium 10 in the Greenland Ice Core Project ice core at Summit, Greenland, *J. Geophys. Res. 102*, 26783-26794.

Zic, M., R. Negrini, and P.E. Wigand (2002), Evidence of synchronous climate change across the Northern Hemisphere between the North Atlantic and the northwestern Great Basin, United States, *Geology 30*, 635–638.

Zimmerman, S.H., S.R. Hemming, D.V. Kent, and S.Y. Searle (2006), Revised chronology for late Pleistocene Mono Lake sediments based on paleointensity correlation to the global reference curve, *Earth Planet. Sci. Lett. 252*, 94-106.

Figure Captions :

824 Figure 1. A. Location map of the MD05-2920 coring site in the Bismarck Sea, on the
825 Papua New Guinea northern margin. B. Location of the marine sediment cores used in
826 this study: MD05-2020 core located North of Papua New Guinea (NPNG), MD04-2811
827 and MD95-2042 cores located on the Portuguese Margin. Location of the GRIP and
828 GISP2 ice cores at Summit (Greenland).

829 Figure 2. A. The $^{10}Be/^{9}Be$ record along core MD05-2920. B. The NRM and ARM
830 intensities are both demagnetized at 30mT AF step along core MD05-2920 and provide a
831 ratio considered as the best Relative Paleointensity proxy. C. $\delta^{18}O$ measured on benthic
832 foraminifer *Uvigerina peregrina* (Tachikawa et al., 2011). D. Chronostratigraphic
833 markers in MD05-2920 sediments, and the depth-age relationship. Green dots are
834 radiocarbon dated levels, and the blue dot is the MIS-3 MIS-4 transition tie point.
835 Between these points, the age model is based on linear interpolation.

836 Figure 3. (a) ^{10}Be deposition flux (10^{6} atoms/cm^{2}/yr) record at Summit (Greenland) in
837 GIPS2 and GRIP ice cores [*Finkel et al.*, 1997; *Yiou et al*., 1997; *Muscheler et al.*, 2005].
838 Authigenic $^{10}Be/^{9}Be$ ratios (10^{-8}) records in the Portuguese Margin (b) and Papua New
839 Guinea (c) sediments.

840 Figure 4. Records of ^{10}Be atmospheric production variations between 20 and 60 ka. Dots
841 correspond to the authigenic $^{10}Be/^{9}Be$ ratios from MD04-2811 (blue dots), MD05-2920
842 (red dots) and MD95-2042 (black dots). In grey, the Greenland ^{10}Be deposition flux
843 variations. All data series are normalized to their own mean values, and plotted on their
844 own chronological scales.

Figure 5. Variations of the ^{10}Be production in the atmosphere during the 20-50 ka period. In red, the authigenic $^{10}Be/^{9}Be$ composite record, and the associated 1σ uncertainties. It is compared with the Greenland ^{10}Be-Flux record (In grey), and its 1000-year smoothed version (black curve). The Greenland record is normalized to its own mean value, and plotted on its own chronological scale (see text).

Figure 6. Calibration of the normalized $^{10}Be/^{9}Be$ (proxy of the normalized ^{10}Be production) values using Virtual Dipole Moments (VDM) values provided by the GEOMAGIA-50 database [*Korhonen et al*., 2008], and the polynomial fit used to derive Virtual Dipole Moments (VDM): $y = 32.973 - 42.156x + 13.921x^2$. The normalized $^{10}Be/^{9}Be$ intermediate and minimum clusters are calculated using values comprised within the « mean ± 1σ » range, and using values less than « mean - 1σ », respectively. Associated error bars correspond to the standard deviation of the values used for averaging. Grey dots indicate normalized dipole moments obtained after application of Elsasser's algorithm [see *Lal,* 1992] on the normalized $^{10}Be/^{9}Be$ data.

Figure 7. ^{10}Be-based VDM reconstruction (in 10^{22} Am^2) and associated 1-sigma uncertainties, compared to paleomagnetic VADM reconstructions (GLOPIS-75 and SINT 800 reference records) over the 20- 50 ka interval. The grey band represents the GLOPIS-75 1 sigma envelop [*Laj et al.,* 2004] plotted on the GICC05 time-scale, and the black curve is the SINT 800 reconstruction [*Guyodo and Valet,* 1999]. Each data series is plotted on its own time scale. The dotted line shows the present-day VADM value of ~8 x 10^{22} $A.m^2$.

867

868

869

870

871

872

873

874

875

876

877

A.

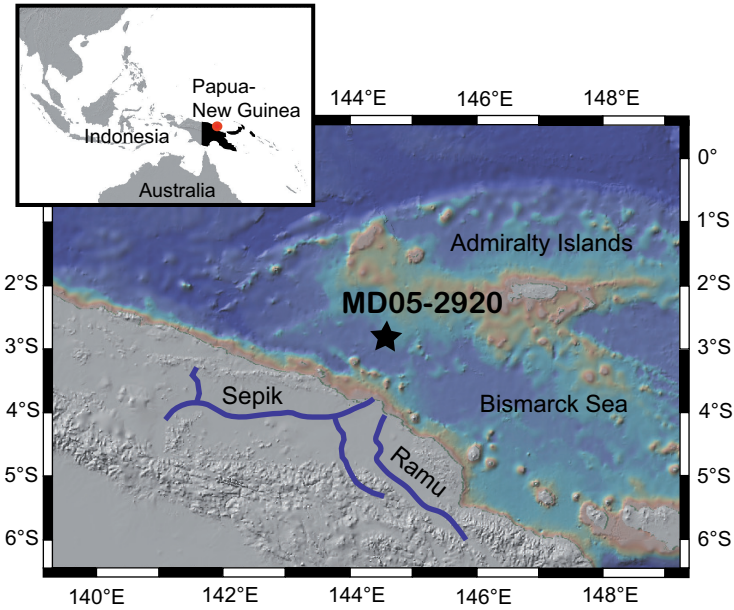
Papua-
New Guinea
Indonesia
Australia
144°E
146°E
148°E
0°
1°S
2°S
3°S
4°S
5°S
6°S
Admiralty Islands
MD05-2920
Sepik
Bismarck Sea
Ramu
140°E
142°E
144°E
146°E
148°E

B.

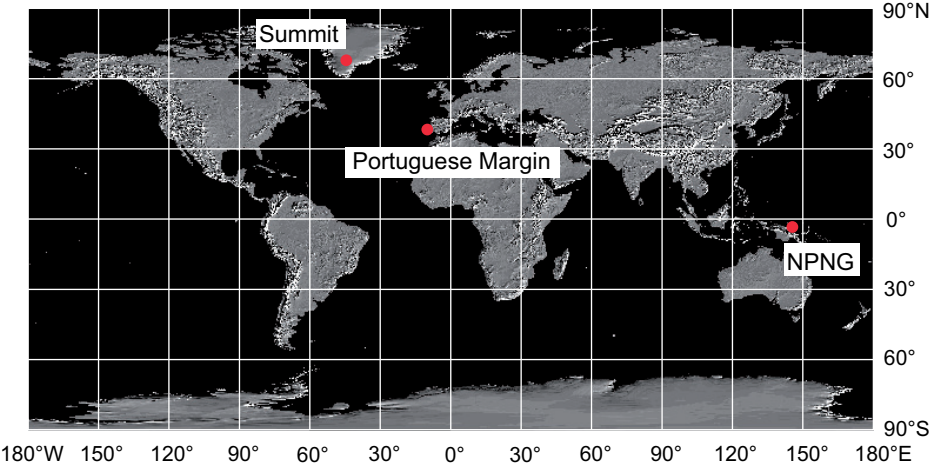
Summit
Portuguese Margin
NPNG
90°N
60°
30°
0°
30°
60°
90°S
180°W
150°
120°
90°
60°
30°
0°
30°
60°
90°
120°
150°
180°E

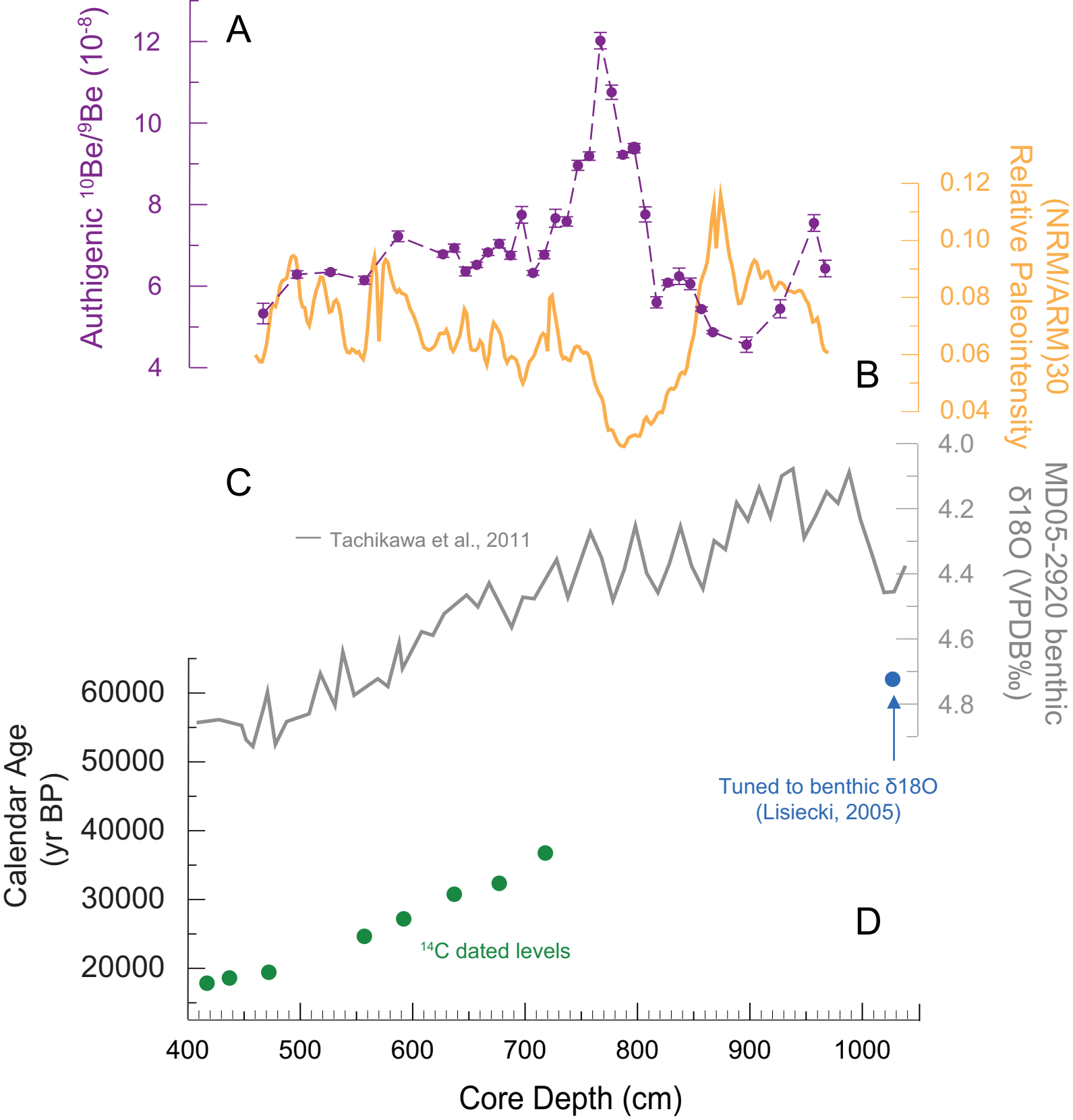
A
Authigenic $^{10}Be/^{9}Be$ (10^{-8})
12
10
8
6
4
B
Relative Paleointensity (NRM/ARM)30
0.12
0.10
0.08
0.06
0.04
C
Tachikawa et al., 2011
MD05-2920 benthic δ18O (VPDB‰)
4.0
4.2
4.4
4.6
4.8
Tuned to benthic δ18O
(Lisiecki, 2005)
D
^{14}C dated levels
Calendar Age
(yr BP)
60000
50000
40000
30000
20000
400
500
600
700
800
900
1000
Core Depth (cm)

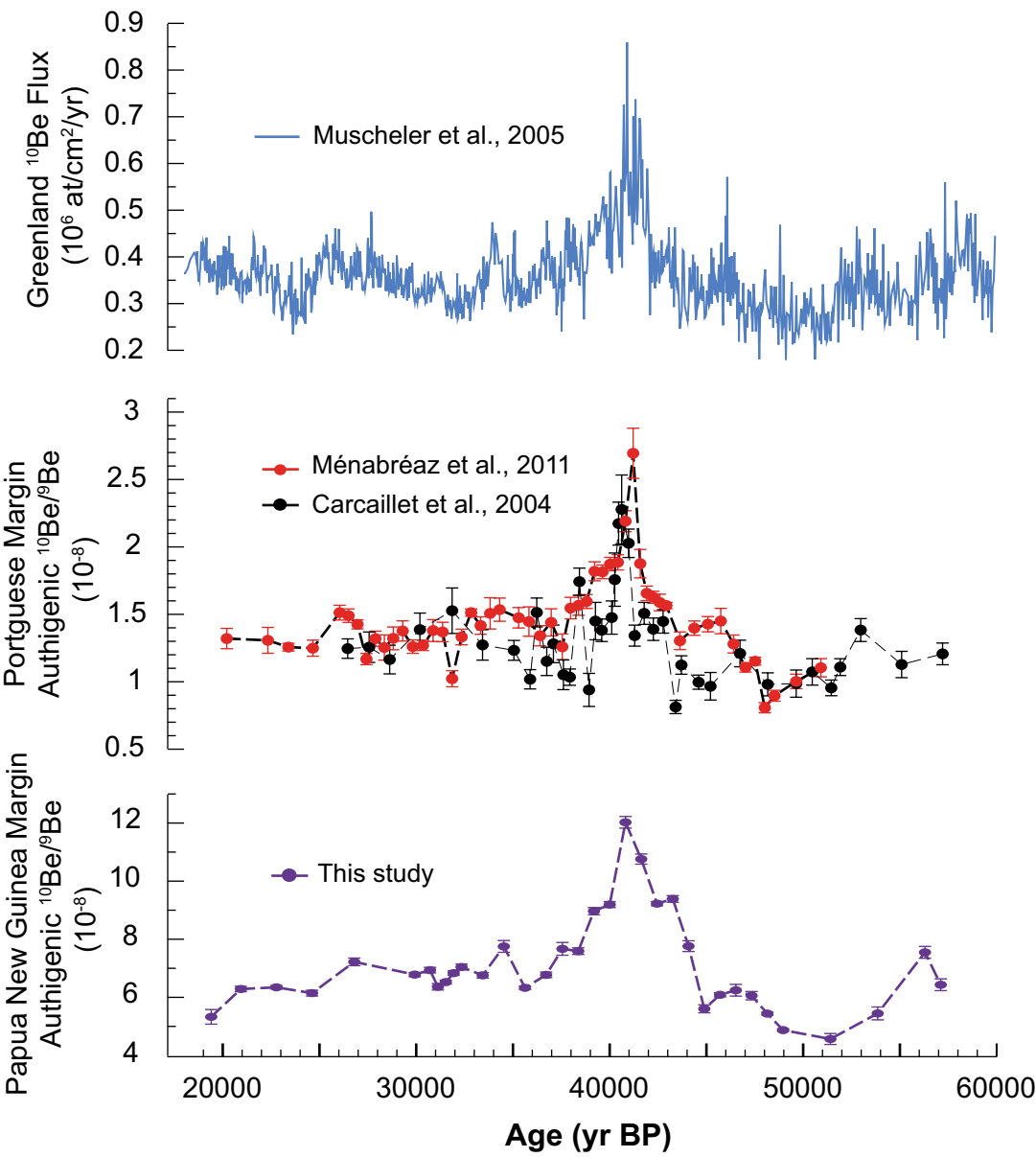
Greenland ^{10}Be Flux
(10^6 at/cm^2/yr)
0.9
0.8
0.7
0.6
0.5
0.4
0.3
0.2
Muscheler et al., 2005
Portguese Margin
Authigenic ^{10}Be/^{9}Be
(10^{-8})
3
2.5
2
1.5
1
0.5
Ménabréaz et al., 2011
Carcaillet et al., 2004
Papua New Guinea Margin
Authigenic ^{10}Be/^{9}Be
(10^{-8})
12
10
8
6
4
This study
20000
30000
40000
50000
60000
Age (yr BP)

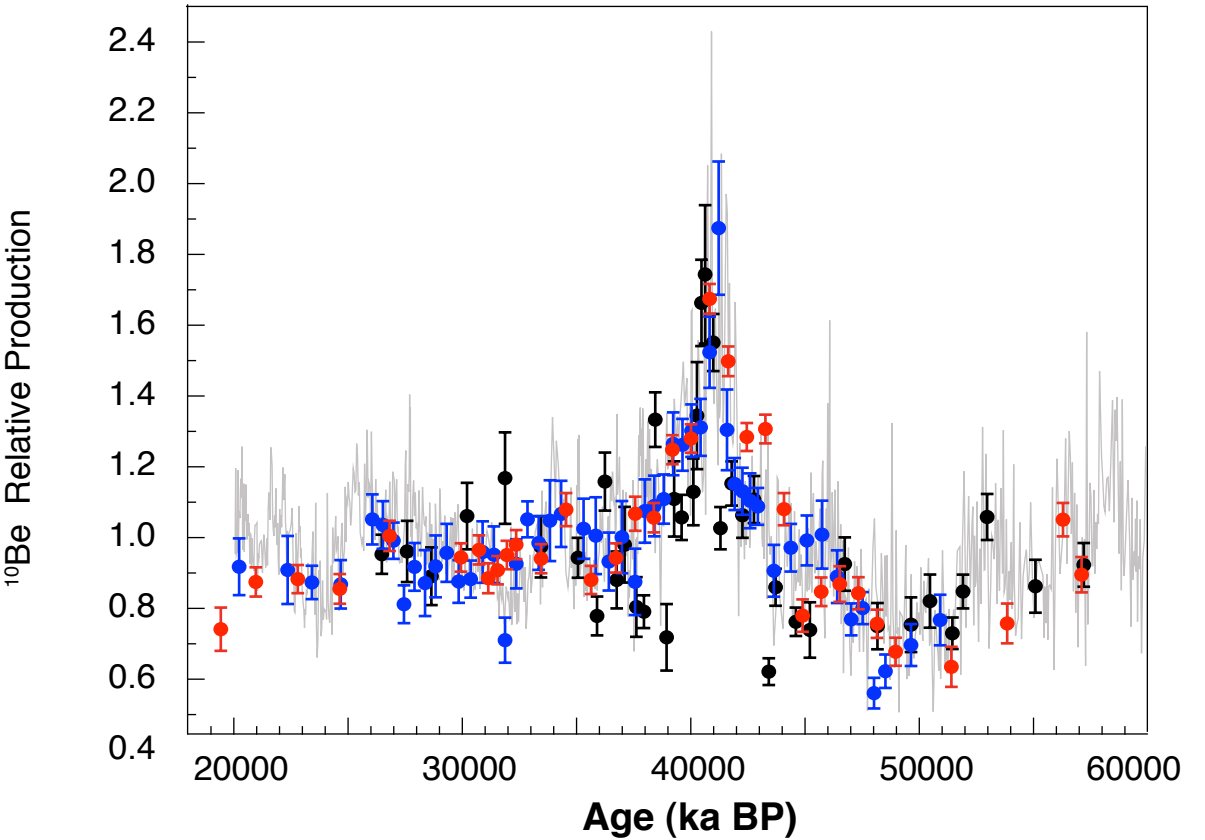
^{10}Be Relative Production
2.4
2.2
2.0
1.8
1.6
1.4
1.2
1.0
0.8
0.6
0.4
20000
30000
40000
50000
60000
Age (ka BP)

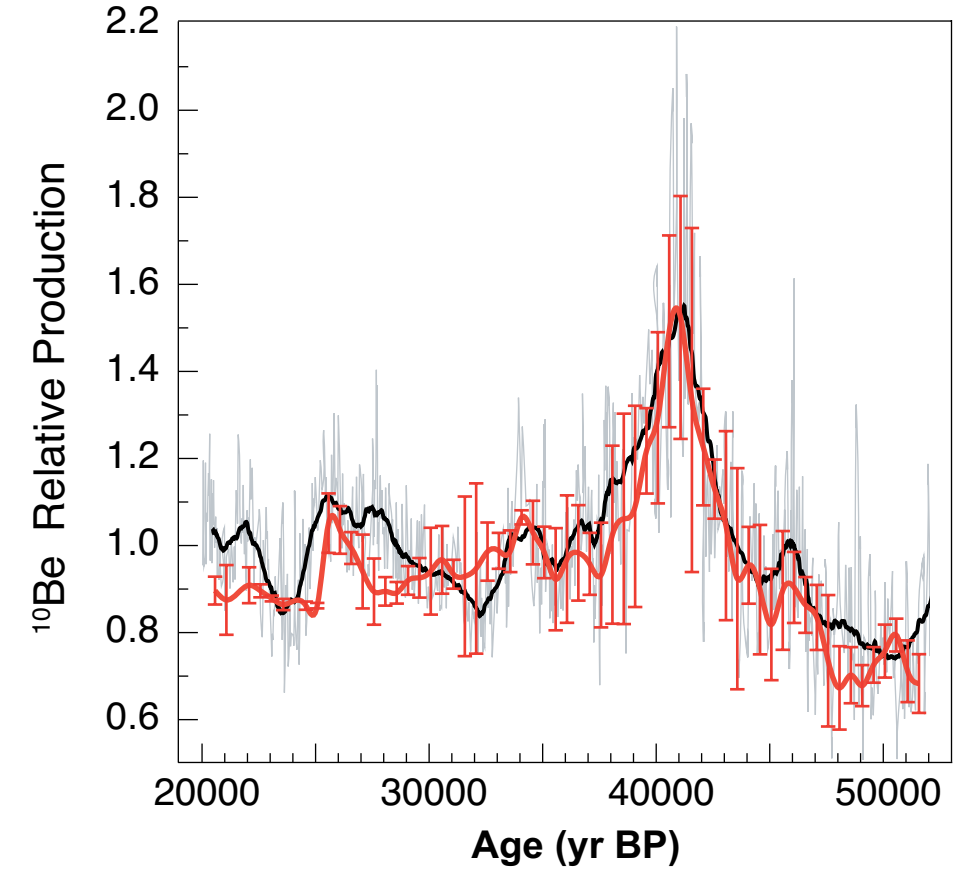
2.2
2.0
1.8
1.6
1.4
1.2
1.0
0.8
0.6
^{10}Be Relative Production
20000
30000
40000
50000
Age (yr BP)

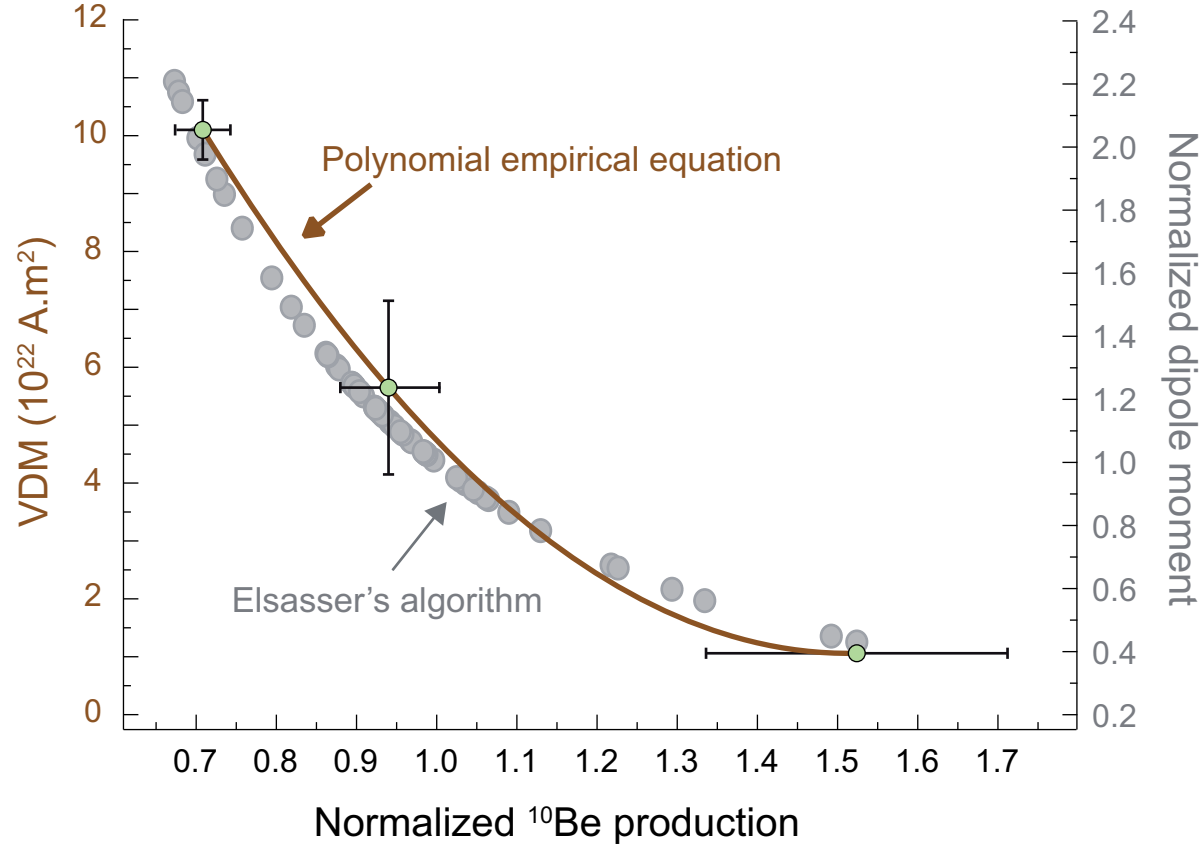
Polynomial empirical equation
Elsasser's algorithm
VDM (10^{22} A.m^2)
Normalized dipole moment
Normalized ^{10}Be production
12
10
8
6
4
2
0
2.4
2.2
2.0
1.8
1.6
1.4
1.2
1.0
0.8
0.6
0.4
0.2
0.7
0.8
0.9
1.0
1.1
1.2
1.3
1.4
1.5
1.6
1.7

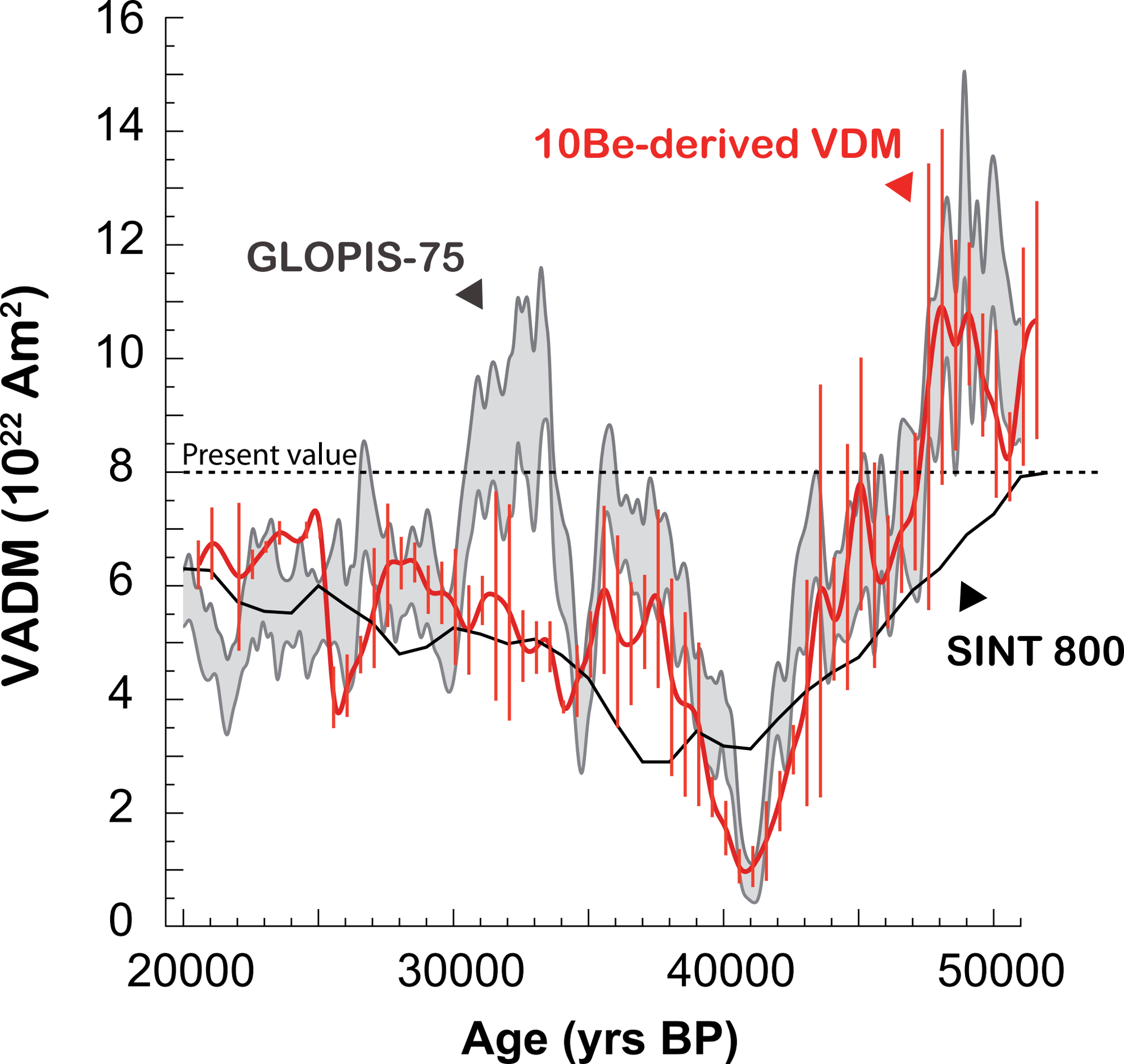
16
14
12
10
8
6
4
2
0
VADM (10^22 Am^2)
10Be-derived VDM
GLOPIS-75
Present value
SINT 800
20000
30000
40000
50000
Age (yrs BP)

Table1: AMS measurements, Be isotopes concentrations and authigenic $^{10}Be/^{9}Be$ ratios of core MD05-2920 samples.

Sample: Core name-sample depth in core (cm)	Age (BP)	Measured $^{10}Be/^{9}Be$ (10^{-11}) *	Decay-corrected authigenic [^{10}Be] (10^{-14}g/g) *	Authigenic [^{9}Be] (10^{-7}g/g) *	Authigenic $^{10}Be/^{9}Be$ (10^{-8}) *
MD05 2920-467	19405	2.134±0.021	0.956±0.009	1.793±0.083	5.33±0.26
MD05 2920-797	20937	3.307±0.034	1.535±0.016	2.442±0.026	6.29±0.10
MD05 2920-527	22777	3.148±0.029	1.475±0.014	2.325±0.006	6.34±0.06
MD05 2920-557	24616	3.246±0.031	1.558±0.015	2.536±0.033	6.15±0.10
MD05 2920-587	26798	2.508±0.024	1.701±0.016	2.355±0.037	7.22±0.14
MD05 2920-627	29925	4.097±0.035	1.723±0.015	2.540±0.017	6.78±0.08
MD05 2920-637	30714	4.094±0.035	1.724±0.015	2.486±0.028	6.94±0.10
MD05 2920-647	31121	3.636±0.033	1.541±0.014	2.423±0.036	6.36±0.11
MD05 2920-657	31529	3.546±0.033	1.457±0.014	2.233±0.010	6.52±0.07
MD05 2920-667	31936	3.604±0.032	1.538±0.014	2.252±0.016	6.83±0.08
MD05 2920-677	32343	3.693±0.034	1.477±0.014	2.098±0.023	7.04±0.10
MD05 2920-687	33436	4.419±0.040	1.717±0.016	2.542±0.028	6.75±0.10
MD05 2920-697	34529	4.386±0.038	1.609±0.014	2.076±0.052	7.75±0.21
MD05 2920-707	35622	3.330±0.030	1.546±0.014	2.445±0.007	6.32±0.06
MD05 2920-717	36715	4.787±0.043	1.763±0.016	2.604±0.030	6.77±0.10
MD05 2920-727	37557	2.910±0.060	1.830±0.038	2.387±0.048	7.67±0.22
MD05 2920-737	38372	3.426±0.030	1.865±0.017	2.458±0.031	7.59±0.12
MD05 2920-747	39187	4.987±0.042	2.104±0.018	2.347±0.026	8.96±0.13
MD05 2920-757	40002	5.540±0.047	2.311±0.020	2.514±0.019	9.19±0.11
MD05 2920-767	40816	4.358±0.028	2.439±0.016	2.029±0.032	12.01±0.21
MD05 2920-777	41631	3.994±0.023	2.274±0.013	2.115±0.033	10.75±0.18
MD05 2920-787	42446	3.662±0.025	2.068±0.014	2.242±0.011	9.22±0.08
MD05 2920-797	43261	4.262±0.028	1.892±0.013	2.016±0.021	9.38±0.12
MD05 2920-807	44075	3.829±0.027	1.627±0.012	2.097±0.048	7.76±0.19
MD05 2920-817	44890	3.077±0.023	1.307±0.010	2.333±0.055	5.60±0.14
MD05 2920-827	45705	2.672±0.019	1.294±0.010	2.127±0.020	6.09±0.08
MD05 2920-837	46520	2.850±0.019	1.335±0.009	2.138±0.068	6.24±0.21
MD05 2920-847	47334	3.419±0.022	1.276±0.009	2.107±0.048	6.06±0.15
MD05 2920-857	48149	2.590±0.019	1.227±0.009	2.257±0.015	5.44±0.06
MD05 2920-867	48964	2.531±0.020	1.222±0.010	2.509±0.008	4.87±0.05
MD05 2920-897	51408	1.645±0.015	1.123±0.010	2.459±0.100	4.57±0.19
MD05 2920-927	53852	2.051±0.016	1.400±0.011	2.572±0.103	5.45±0.23
MD05 2920-957	56297	2.834±0.021	1.549±0.012	2.053±0.054	7.55±0.21
MD05 2920-967	57111	3.181±0.023	1.543±0.011	2.398±0.074	6.43±0.21
mean ± std. dev.			1.618±0.397	2.303±0.202	**7.07±1.62**
mean ± SDOM					**7.07±0.28**

* errors are 1 sigma, and rounded to the higher value. Sample depths are corrected from the 30 cm surface sediment void.

Table 2: *Chronological data for MD05-2920 age model construction.*

Sample depth in core MD05-2920 (cm) [a]	^{14}C Age [b] (^{14}C yr BP)	Calibrated Age (yr BP)	Method
40	2610 ± 35	2151 ± 206	^{14}C AMS ages, INTCAL09 *
80	4445 ± 35	4553 ± 271	^{14}C AMS ages, INTCAL09 *
119	6040 ± 40	6463 ± 191	^{14}C AMS ages, INTCAL09 *
198	8965 ± 45	9544 ± 251	^{14}C AMS ages, INTCAL09 *
253	10120 ± 35	11000 ± 252	^{14}C AMS ages, INTCAL09 *
302	11835 ± 45	13289 ± 196	^{14}C AMS ages, INTCAL09 *
322	12525 ± 40	13973 ± 267	^{14}C AMS ages, INTCAL09 *
352	12575 ± 45	14146 ± 396	^{14}C AMS ages, INTCAL09 *
417	15130 ± 60	18375 ± 130	^{14}C AMS ages, INTCAL09 *
437	15710 ± 60	19405 ± 197	^{14}C AMS ages, INTCAL09 *
472	16710 ± 60	19405 ± 197	^{14}C AMS ages, INTCAL09 *
557	21030 ± 90	24616 ± 409	^{14}C AMS ages, INTCAL09 *
592	22840 ± 90	27162 ± 609	^{14}C AMS ages, INTCAL09 *
637	26430 ± 130	30714 ± 557	^{14}C AMS ages, INTCAL09 *
677	28560 ± 160	32343 ± 715	^{14}C AMS ages, INTCAL09 *
718	32520 ± 240	36824 ± 623	^{14}C AMS ages, INTCAL09 *
1027		62000	Tuned to benthic δ^{18}O **

[a] All depths in core MD05-2920 are corrected for a top-core 30 cm void.

[b] All ^{14}C ages were determined by *Tachikawa et al.* [2011], and corrected for a regional reservoir age of 420 ± 60 years given by *McGregor et al.* [2008]. Errors are 2-sigma.

* *Reimer et al.* [2009]

** *Lisiecki and Raymo* [2005], *Tachikawa et al.* [2011].

Table 3: Authigenic $^{10}Be/^{9}Be$ marine stacked record, and corresponding ^{10}Be-based VDM record.

Age (BP)	Authigenic $^{10}Be/^{9}Be$ stack (normalized data)	VDM (10^{22} A.m^2)
20572	0.90 ± 0.03	6.4 ± 0.4
21072	0.87 ± 0.04	6.7 ± 0.6
22072	0.91 ± 0.10	6.2 ± 1.3
22572	0.90 ± 0.02	6.4 ± 0.3
23072	0.88 ± 0.01	6.7 ± 0.1
23572	0.86 ± 0.01	6.9 ± 0.2
24572	0.86 ± 0.01	7,0 ± 0.1
25072	0.86 ± 0.01	7,0 ± 0.1
25572	1.05 ± 0.07	4,0 ± 0.5
26072	1.04 ± 0.07	4.2 ± 0.6
26572	1.00 ± 0.04	4.8 ± 0.3
27072	0.94 ± 0.09	5.6 ± 1.1
27572	0.90 ± 0.08	6.4 ± 1.1
28072	0.89 ± 0.04	6.4 ± 0.5
28572	0.89 ± 0.02	6.4 ± 0.4
29072	0.92 ± 0.03	5.9 ± 0.4
29572	0.93 ± 0.04	5.9 ± 0.6
30072	0.94 ± 0.09	5.6 ± 1,0
30572	0.97 ± 0.07	5.2 ± 0.8
31072	0.93 ± 0.04	5.7 ± 0.4
31572	0.93 ± 0.15	5.8 ± 1.8
32072	0.95 ± 0.16	5.5 ± 1.9
32572	0.99 ± 0.06	4.9 ± 0.6
33072	0.99 ± 0.05	4.9 ± 0.5
33572	0.99 ± 0.04	4.9 ± 0.4
34072	1.06 ± 0.02	3.9 ± 0.1
34572	1.03 ± 0.08	4.3 ± 0.6

35072	0.98 ± 0.06	5,0 ± 0.6
35572	0.92 ± 0.12	5.9 ± 1.5
36072	0.97 ± 0.16	5.2 ± 1.7
36572	0.98 ± 0.11	5,0 ± 1.1
37072	0.96 ± 0.07	5.4 ± 0.8
37572	0.93 ± 0.13	5.8 ± 1.6
38072	1.02 ± 0.20	4.4 ± 1.7
38572	1.06 ± 0.22	3.9 ± 1.6
39072	1.09 ± 0.22	3.6 ± 1.4
39572	1.22 ± 0.09	2.3 ± 0.4
40072	1.29 ± 0.18	1.7 ± 0.5
40572	1.49 ± 0.21	1.1 ± 0.3
41072	1.52 ± 0.26	1.1 ± 0.4
41572	1.33 ± 0.31	1.5 ± 0.7
42072	1.23 ± 0.15	2.2 ± 0.5
42572	1.13 ± 0.08	3.1 ± 0.4
43072	1.05 ± 0.25	4.2 ± 2,0
43572	0.92 ± 0.28	5.9 ± 3.6
44072	0.95 ± 0.10	5.4 ± 1.1
44572	0.09 ± 0.15	6.3 ± 2.2
45072	0.82 ± 0.12	7.8 ± 2.2
45572	0.90 ± 0.13	6.4 ± 1.8
46072	0.90 ± 0.07	6.2 ± 1,0
46572	0.86 ± 0.07	7,0 ± 1.1
47072	0.83 ± 0.07	7.5 ± 1.2
47572	0.74 ± 0.15	9.5 ± 3.9
48072	0.67 ± 0.10	10.9 ± 3.1
48572	0.70 ± 0.06	10.2 ± 1.9
49072	0.68 ± 0.04	10.8 ± 1.3
49572	0.73 ± 0.04	9.7 ± 1.1
50072	0.76 ± 0.06	9,0 ± 1.5

50572	0.79 ± 0.04	8.3 ± 0.8
51072	0.71 ± 0.07	10,0 ± 1.9
51572	0.68 ± 0.07	10.7 ± 2.1

errors are 1-sigma